JOURNAL OF PETROLOGY

Journal of Petrology, 2016, Vol. 57, No. 6, 1199–1222
doi: 10.1093/petrology/egw037
Original Article

OXFORD

Garnet and Spinel Oxybarometers: New Internally Consistent Multi-equilibria Models with Applications to the Oxidation State of the Lithospheric Mantle

William G. R. Miller[1], Tim J. B. Holland[1]* and Sally A. Gibson[1]

[1]Department of Earth Sciences, University of Cambridge, Downing Street, Cambridge CB2 3EQ, UK

*Corresponding author: Telephone +44 (0)1223 333466. E-mail: tjbh@cam.ac.uk

Received August 18, 2015; Accepted May 31, 2016

ABSTRACT

New thermodynamic data for skiagite garnet ($Fe_3Fe_2^{3+}Si_3O_{12}$) are derived from experimental phase-equilibrium data that extend to 10 GPa and are applied to oxybarometry of mantle peridotites using a revised six-component garnet mixing model. Skiagite is more stable by 12 kJ mol^{-1} than in a previous calibration of the equilibrium 2 skiagite = 4 fayalite + ferrosilite + O_2, and this leads to calculated oxygen fugacities that are higher (more oxidized) by around 1–1·5 log f_{O_2} units. A new calculation method and computer program incorporates four independent oxybarometers (including 2 pyrope + 2 andradite + 2 ferrosilite = 2 grossular + 4 fayalite + 3 enstatite + O_2) for use on natural peridotite samples to yield optimum log f_{O_2} estimates by the method of least squares. These estimates should be more robust than those based on any single barometer and allow assessment of possible disequilibrium in assemblages. A new set of independent oxybarometers for spinel-bearing peridotites is also presented here, including a new reaction 2 magnetite + 3 enstatite = 3 fayalite + 3 forsterite + O_2. These recalibrations combined with internally consistent *PT* determinations for published analyses of mantle peridotites with analysed Fe_2O_3 data for garnets, from both cratonic (Kaapvaal, Siberia and Slave) and circumcratonic (Baikal Rift) regions, provide revised estimates of oxidation state in the lithospheric mantle. Estimates of log f_{O_2} for spinel assemblages are more reduced than those based on earlier calibrations, whereas garnet-bearing assemblages are more oxidized. Importantly, this lessens considerably the difference between garnet and spinel oxybarometry that was observed with previous published calibrations.

Key words: peridotite; oxybarometry; igneous petrology; mantle

INTRODUCTION

The redox state of the Earth's mantle is of fundamental importance in understanding how it melts, how the abundance and disposition of carbon-bearing minerals and fluids vary at greater depths, where diamonds form, and the depths at which they entrap a variety of silicate and oxide inclusions (Harte & Cayser, 2007; Frost & McCammon, 2008; Dasgupta & Hirschmann, 2010; Foley, 2010; Harte, 2010; Stagno *et al.*, 2013). Most attempts to determine mantle log f_{O_2} are based on the pioneering calibration of Gudmundsson & Wood (1995), who used an oxygen barometer based on the reaction

$$2ski = 4fa + fs + O_2 \quad (1)$$

where ski is skiagite ($Fe_3Fe_2^{3+}Si_3O_{12}$), fa is fayalite (Fe_2SiO_4) and fs is ferrosilite ($Fe_2Si_2O_6$). Accounting for the activities of ski, fa and fs in garnet, olivine and orthopyroxene allows determination of the oxygen activity, usually expressed in terms of log f_{O_2}. More recently this calibration has been questioned by Stagno

et al. (2013), who proposed an alternative oxybarometer based on the equilibrium of Luth *et al.* (1990):

$$2\text{py} + 2\,\text{andr} + 2\ \text{fs} = 2\,\text{gr} + 4\ \text{fa} + 3\ \text{en} + \text{O}_2 \quad (2)$$

where py is pyrope ($Mg_3Al_2Si_3O_{12}$), andr is andradite ($Ca_3Fe_2Si_3O_{12}$), gr is grossular ($Ca_3Al_2Si_3O_{12}$), and en is enstatite ($Mg_2Si_2O_6$). On the basis of their own oxygen sensor measurements, Stagno *et al.* (2013) suggested that reaction (2), calibrated using the thermodynamic data of Holland & Powell (2011), provides an oxybarometer that satisfies the available data better than reaction (1). Stagno *et al.* (2013) showed that calculations based on reaction (1) deviated from their experiments by 0·5–2 log units in which log f_{O_2} was measured by an Ir–Fe sensor, with the largest deviations occurring at the highest pressures (6–7 GPa). Here we show that there was an error in the original thermodynamic calibration of reaction (1) and proceed to derive new thermodynamic data for skiagite that allow reconciliation between the two barometers and pave the way to using a multi-reaction approach involving optimization of log f_{O_2} by least squares. This should help determine whether minerals in an assemblage have equilibrated effectively and hence should provide more robust estimates for log f_{O_2}.

The problem with the original calibration of reaction (1) lies in an error in the Gibbs free energy adopted for that reaction by Gudmundsson & Wood (1995). In their analysis the Gibbs energy change for reaction (1) was estimated as 133·3 kJ at 1 bar and 1100°C (log $K_1 =$ –5·07), this value being based on the calculations of Woodland & O'Neill (1993) on the reaction involving hercynite (hc, $FeAl_2O_4$):

$$\text{ski} + \text{hc} = \text{alm} + \text{mt} \quad (3)$$

for which they derived a Gibbs energy of –69·3 kJ. This led them, through a sequence of calculations based on thermodynamic data from Holmes *et al.* (1986) and Holland & Powell (1990), to deduce the free energy of reaction (4) involving quartz (qz, SiO_2) and iron metal (Fe)

$$\text{ski} = 5\text{Fe} + 3\text{q} + 3\text{O}_2 \quad (4)$$

as 981·0 kJ at 1 bar and 1100°C. This value was used by Gudmundsson & Wood (1995) in their derivation of the free energy for reaction (1). A recalculation of the free energy of reaction (4) (see Appendix), with the data sources used by Woodland & O'Neill (1993), leads to a significantly smaller value (970·4 kJ), which in turn causes the oxybarometer to be systematically in error. The newer thermodynamic data of Holland & Powell (2011), as opposed to those of Holland & Powell (1990), lead to essentially the same value (969·0 kJ) and therefore a reassessment and recalibration of reaction (1) is warranted.

Reaction (1) requires thermodynamic data for skiagite that may be combined with existing data for fayalite, ferrosilite and oxygen. The following three equilibria, involving hc (hercynite, $FeAl_2O_4$), alm (almandine, $Fe_3Al_2Si_3O_{12}$), frw (ferroringwoodite, Fe_2SiO_4), mt (magnetite, Fe_3O_4), and coe (coesite, SiO_2) are involved in the experimental data of Woodland & O'Neill (1993):

$$\text{ski} + \text{hc} = \text{alm} + \text{mt} \quad (3)$$

$$\text{ski} = \text{frw} + \text{mt} + 2\ \text{coe} \quad (5)$$

$$\text{frw} + \text{hc} + 2\ \text{coe} = \text{alm}. \quad (6)$$

It should be noted that reaction (6) is a linear combination of (3) and (5) but can provide a test of consistency between the experimental results of Woodland & O'Neill (1993) and the thermodynamic data of Holland & Powell (2011) that is independent of skiagite. Woodland & O'Neill (1993) used only reaction (3) above to derive thermodynamic data for skiagite, because the spinel in their lower pressure experiments (<45 kbar) was dominantly a hercynite–magnetite solid solution, whereas in the higher pressure runs increasing amounts of ferroringwoodite component were present. Availability of thermodynamic data for ferroringwoodite in the more recent dataset of Holland & Powell (2011) allows use of reaction (5) as an additional check on internal consistency of the data. The lowest pressure studied by Woodland & O'Neill (1993) involved quartz rather than coesite, and so, although the results reported here involve coesite, quartz was used in place of coesite in our analysis of the 27 kbar runs.

Clearly, use of reactions (3), (5) and (6) requires a solution model for ternary hc–mt–frw spinel. In this study we assume complete disorder in spinel and use the three-site model simplification as proposed by Bryndzia & Wood (1990) and Wood et al. (1990). Several lines of evidence suggest that this is reasonable and adequate for the purposes of this study: first, a binary mt–hc spinel using $W_{hc,mt} = 38$ kJ allows calculation of the solvus of Turnock & Eugster (1962) almost perfectly; second, O'Neill & Navrotsky (1983) in their treatment of order–disorder in spinels also found that $W_{hc,mt} = 38$ kJ was required to fit the solvus using their more complex model; third, the calorimetry performed by Navrotsky (1986) on $MgFe_2O_4$–$MgAl_2O_4$ demands a value for $W_{hc,mt}$ of 40·4 ± 4 kJ, which matches closely that found here for the analogous binary $FeFe_2O_4$–$FeAl_2O_4$; fourth, the activity of hercynite and magnetite in a binary spinel at 1300°C has been experimentally measured by Petric *et al.* (1981), and the calculated activities of both hercynite and magnetite are close to 0·5 at $X_{mt} = 0{\cdot}5$ as in the experimental determination; finally, the ternary spinel model when fitted to the three reactions (3), (5) and (6) using the experiments of Woodland & O'Neill (1993) yields thermodynamic data that are entirely consistent with the dataset of Holland & Powell (2011), as shown below. These considerations suggest that the simple spinel model that we have used is an adequate approximation for this system at these conditions.

RECALIBRATION OF THE SKIAGITE BAROMETER

Woodland & O'Neill (1993) equilibrated garnet and spinel experimentally at 1100°C and analysed their results using equilibrium (3). They deduced the free energy of skiagite from their data, using only experiments at pressures below 45 kbar (where the spinels contain very little of the frw end-member). Woodland & O'Neill (1993) also assumed that, at these conditions, garnet and spinel form binary alm–ski and mt–hc solid solutions. We have extended their calibration by incorporating all of their high-pressure data using the ternary mt–hc–frw solution model for spinel outlined above. For reaction (3) the equilibrium constant is

$$K_{(3)} = \frac{a_{\mathrm{alm}}\, a_{\mathrm{mt}}}{a_{\mathrm{ski}}\, a_{\mathrm{hc}}}.$$

In the binary alm–ski garnet (gt), with mixing on only the Y sites, the ideal activities (id) are given as

$$a^{\mathrm{id}}_{\mathrm{ski}} = (X^{\mathrm{gt}}_{\mathrm{Fe}^{3+},\mathrm{Y}})^2 = X^2_{\mathrm{ski}}, \quad a^{\mathrm{id}}_{\mathrm{alm}} = (X^{\mathrm{gt}}_{\mathrm{Al,Y}})^2 = X^2_{\mathrm{alm}}$$

and in a ternary spinel (sp) the ideal mixing activities become

$$a^{\mathrm{id}}_{\mathrm{mt}} = \tfrac{27}{4} X^{\mathrm{sp}}_{Fe}(X^{\mathrm{sp}}_{\mathrm{Fe}^{3+}})^2, a^{\mathrm{id}}_{\mathrm{hc}} = \tfrac{27}{4} X^{\mathrm{sp}}_{\mathrm{Fe}}(X^{\mathrm{sp}}_{\mathrm{Al}})^2,$$
$$a^{\mathrm{id}}_{\mathrm{frw}} = \tfrac{27}{4} X^{\mathrm{sp}}_{\mathrm{Si}}(X^{\mathrm{sp}}_{\mathrm{Fe}})^2.$$

Adding in non-ideality, the usual condition of equilibrium at 1 bar and 1100°C (1373 K) may be written as

$$0 = \Delta G_{(3)1,1373} + P\Delta V_{(3)} + \mathrm{R}T\ln\frac{a^{\mathrm{id}}_{\mathrm{mt}}(a^{\mathrm{id}}_{\mathrm{alm}})^2}{a^{\mathrm{id}}_{\mathrm{hc}}(a^{\mathrm{id}}_{\mathrm{ski}})^2} + \mathrm{R}T\ln\gamma_i.$$

where $\Delta G_{(3)1,1373}$ is the Gibbs free energy of reaction (3) at 1 bar and 1373 K and the $\sum \mathrm{R}T\ln\gamma_i$ terms come from a regular solution model (see Appendix) in both garnet (ski, alm) and spinel (hc, mt, frw), giving for reaction (3)

$$0 = \Delta G_{(3)1,1373} + P\Delta V_{(3)} + \mathrm{R}T\ln\frac{a^{\mathrm{id}}_{\mathrm{mt}}(a^{\mathrm{id}}_{\mathrm{alm}})^2}{a^{\mathrm{id}}_{\mathrm{hc}}(a^{\mathrm{id}}_{\mathrm{ski}})^2} + W_{\mathrm{alm,ski}}(2p_{\mathrm{ski}} - 1) + W_{\mathrm{hc,mt}}(p_{\mathrm{hc}} - p_{\mathrm{mt}}) + p_{\mathrm{frw}}\Delta W$$

where $\Delta W = (W_{\mathrm{frw,mt}} - W_{\mathrm{hc,frw}})$, and p_i is the proportion of end-member *i*. The end-member proportions are as follows: $p_{\mathrm{ski}} = X^{\mathrm{gt}}_{\mathrm{ski}}$, $p_{\mathrm{hc}} = \frac{3}{2}X^{\mathrm{sp}}_{\mathrm{Al}}$, $p_{\mathrm{mt}} = \frac{3}{2}X^{\mathrm{sp}}_{\mathrm{Fe}^{3+}}$ and $p_{\mathrm{frw}} = 3X^{\mathrm{sp}}_{\mathrm{Si}}$. The data of Woodland & O'Neill (1993) allow evaluation of the activity terms, and $\Delta V_{(3)}$ is taken as approximately –0·205 kJ kbar^{-1} (linearizing the data in Table 1 at the pressures and temperatures of the experiments). We can take $W_{\mathrm{alm,ski}} = 2{\cdot}0$ kJ, under the assumption that Al–Fe^{3+} mixing is the same as in grossular–andradite (Holland & Powell, 2011; see Appendix), and $W_{\mathrm{hc,mt}} = 38$ kJ as described above. Plotting

$$-\mathrm{R}T\ln\frac{a^{\mathrm{id}}_{\mathrm{mt}}(a^{\mathrm{id}}_{\mathrm{alm}})^2}{a^{\mathrm{id}}_{\mathrm{hc}}(a^{\mathrm{id}}_{\mathrm{ski}})^2} + 0{\cdot}205P - 38(p_{\mathrm{hc}} - p_{\mathrm{mt}}) - 2(2p_{\mathrm{ski}} - 1)$$

against p_{frw} yields a slope of ΔW and intercept of $\Delta G_{(3)1,1373}$, thus providing a rapid visual estimate for the free energy of skiagite at this temperature (Fig. 1). The data at pressures greater than 45 kbar, disregarded in the analysis of Woodland & O'Neill (1993), are represented in Fig. 1 by values of $p_{\mathrm{frw}} > 0{\cdot}1$ and are clearly required in providing a sufficient range to determine a slope, and hence a value for ΔW.

Additionally, reaction (5) provides further endorsement for the skiagite free energy from the experiments of Woodland & O'Neill (1993). The equilibrium condition for reaction (5) is

$$0 = \Delta G_{(5)1,1373} + P\Delta V_{(5)} + \mathrm{R}T\ln\frac{a^{\mathrm{id}}_{\mathrm{mt}}a^{\mathrm{id}}_{\mathrm{frw}}}{a^{\mathrm{id}}_{\mathrm{ski}}} + W_{\mathrm{alm,ski}}(1 - p_{\mathrm{ski}})^2 + W_{\mathrm{hc,mt}}p_{\mathrm{hc}}(1 - 2p_{\mathrm{mt}}) + W_{\mathrm{frw,mt}}[1 - 2p_{\mathrm{frw}}(p_{\mathrm{hc}} + p_{\mathrm{mt}})] + \Delta W(2p_{\mathrm{frw}}p_{\mathrm{hc}} - p_{\mathrm{hc}})$$

which allows simultaneous determination of both $W_{\mathrm{frw,mt}}$ and the free energy of skiagite. Furthermore, reactions (3) and (5) are linearly related by the equilibrium (6) frw + hc + 2 coe = alm, for which the data in Holland & Powell (2011) provide a constraining value of $\Delta G_{(6)1,1373} = -32{\cdot}1$ kJ. All three equilibria were therefore fitted to the experimental data simultaneously, using THERMOCALC (Powell & Holland, 1988) to generate an updated version of the Holland & Powell (2011) dataset. Thermal expansion and compressibility for all end-members were incorporated (see Table 1). The best fit to all of the data yields

$$\Delta W = 45 \pm 12\ \mathrm{kJ}$$
$$W_{\mathrm{frw,mt}} = 23 \pm 8{\cdot}5\ \mathrm{kJ}$$
$$W_{\mathrm{hc,frw}} = -22 \pm 8{\cdot}5\ \mathrm{kJ}$$
$$\Delta G_{(3)1,1373} = -69{\cdot}5 \pm 1{\cdot}1\ \mathrm{kJ}$$
$$\Delta G_{(5)1,1373} = -37{\cdot}4 \pm 1{\cdot}1\ \mathrm{kJ}.$$

Experimental data for reaction (3) fit the model remarkably well, yielding a value for the free energy at 1 bar and 1373 K of –69·5 kJ, which is in near-perfect agreement with the earlier analysis of Woodland & O'Neill (1993). This is unsurprising, given that both studies use essentially the same value of $W_{\mathrm{hc,mt}} = 38$ kJ, and at the pressures of the Woodland & O'Neill (1993) analysis (<45 kbar) the spinels are close to the binary hercynite–magnetite. However, the newly derived free energy for reaction (1) differs from that used by Gudmundsson & Wood (1995) by over 24 kJ, resulting in log K_1 values that are more positive by 1 log unit than those used in the oxygen barometer calibration by Gudmundsson & Wood (1995). Thus the apparent agreement between the derived barometer expression and the oxygen sensor experiments of Gudmundsson & Wood (1995) is fortuitous. Oxygen fugacities that are 1 log unit more oxidizing than those in the literature appear to be in very good agreement with the measured and calculated bulk Fe_2O_3 contents of mantle peridotites (Jennings & Holland, 2015, fig. 14). The new free

Table 1. Thermodynamic data used in this study

	H	sd(*H*)	*S*	*V*	*a*	*b*	*c*	*d*	a_0	K_0	K_0'
fo	–2172·64	0·54	95·10	4·366	0·2333	0·1494	–603·8	–1·8697	2·85	1285·0	3·84
fa	–1477·94	0·64	151·00	4·631	0·2011	1·7330	–1960·6	–0·9009	2·82	1256·0	4·68
py	–6282·03	1·00	269·50	11·313	0·6335	0	–5196·1	–4·3152	2·37	1743·0	4·05
alm	–5261·08	1·21	342·00	11·525	0·6773	0	–3772·7	–5·0440	2·12	1900·0	2·98
gr	–6642·99	1·38	255·00	12·535	0·6260	0	–5779·2	–4·0029	2·20	1720·0	5·53
andr	–5769·28	1·47	316·40	13·204	0·6386	0	–4955·1	–3·9892	2·86	1588·0	5·68
knor	–5706·17	2·17	302·00	11·738	0·6130	0·3606	–4178·0	–3·7294	2·37	1534·0	4·34
ski	–4332·16	1·92	403·40	12·144	0·6899	0	–2948·6	–5·0303	2·85	1574·0	6·70
uv	–6057·65	1·62	320·90	13·077	0·6051	0·3606	–4760·6	–3·4171	2·20	1620·0	4·70
en	–3090·25	0·63	132·50	6·262	0·3562	–0·2990	–596·9	–3·1853	2·27	1059·0	8·65
fs	–2388·92	0·76	189·90	6·592	0·3987	–0·6579	1290·1	–4·0580	3·26	1010·0	4·08
sp	–2301·22	0·79	82·00	3·978	0·2229	0·6127	–1686·0	–1·5510	1·93	1922·0	4·04
herc	–1953·18	0·80	113·90	4·075	0·2167	0·5868	–2430·2	–1·1783	2·06	1922·0	4·04
mt	–1114·85	0·90	146·90	4·452	0·2625	–0·7205	–1926·2	–1·6557	3·71	1857·0	4·05
frw	–1471·98	0·72	140·00	4·203	0·1668	4·2610	–1705·4	–0·5414	2·22	1977·0	4·92
q	–910·70	0·26	41·43	2·269	0·0929	–0·0642	–714·9	–0·7161	0	730·0	6·00
coe	–906·98	0·26	39·60	2·064	0·1078	–0·3279	–190·3	–1·0416	1·23	979·0	4·19
iron	0·00	0·00	27·09	0·709	0·0462	0·5159	723·1	–0·5562	3·56	1640·0	5·16
O_2	0·00	0·00	205·20	0	0·0483	–0·0691	499·2	–0·4207	0	0	0

End-member names correspond to those of Holland & Powell (2011). *H* is the regressed enthalpy of formation from the elements at 1 bar and 298 K; sd(*H*) is one standard deviation on the enthalpy of formation; *S* is the entropy; *V* the volume (all properties at 1 bar and 298 K); *a*, *b*, *c* and *d* are the coefficients in the heat capacity polynomial $C_p = a + bT + cT^{-2} + dT^{-1/2}$; a_0 and K_0 are thermal expansion and bulk modulus at 298 K; K_0' is the first derivative of bulk modulus at 298 K. Units: *H*, kJ; *S*, J K^{-1}; *V*, kJ $kbar^{-1}$; C_p, kJ K^{-1}; a_0, T^{-1}; K_0, kbar. It should be noted that $C_p(b)$ and a_0 need to be multiplied by 10^{-5}. [See Holland & Powell (2011) for further information on the dataset including details of unchanged order–disorder parameters for sp, herc, mt, iron, q.] Data sources for end-members changed since Holland & Powell (2011) are as follows. ski: *V*, Woodland & O'Neill (1993); K_0, K_0', Woodland *et al.* (1999); *S*, C_p, a_0, estimated from gr, andr and alm. alm, *S*, C_p, Dachs *et al.* (2012). knor: *S*, reduced after Wijbrans *et al.* (2014). uv: *S*, *V*, Klemme *et al.* (2005); C_p, estimated from gr, esk and cor; a_0, as gr; K_0, K_0', Leger *et al.* (1990).

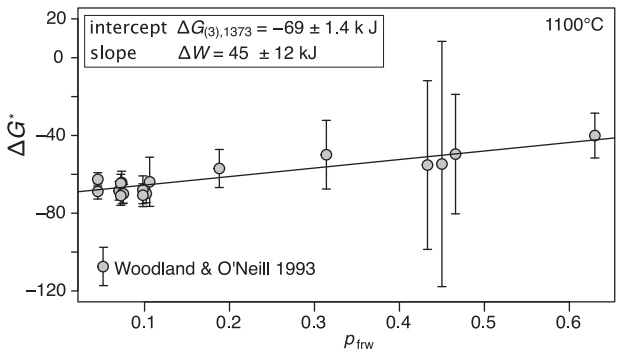

Fig. 1. The data of Woodland & O'Neill (1993) used to calibrate skiagite properties, according to reaction (3). The plot is of $\Delta G* = -RT\ln\frac{a_{mt}^{id}(a_{alm}^{id})^2}{a_{hc}^{id}(a_{ski}^{id})^2} + 0{\cdot}205P - 38(p_{hc} - p_{mt}) - 2(2p_{ski} - 1)$ against p_{frw}, where p_{frw} is the proportion of ferrroringwoodite in spinel. The line has slope $\Delta W = (W_{frw,mt} - W_{hc,frw})$ and intercept $\Delta G_{(3)1,1373}$. Woodland & O'Neill (1993) used only the data for $p_{frw} < 0{\cdot}1$ in their analysis (see text for further explanation).

energies of reaction are found to be non-linear in pressure and temperature and are fitted with a simple polynomial whose coefficients are given in the Appendix. Because the magnitudes of the mixing energy terms in garnet, particularly the cross-site or reciprocal reaction terms, contribute significantly to the application of the barometer they require further discussion and assessment. It should be stressed that inclusion of reaction (5) makes no discernible difference to the derived skiagite free energy, but coupled with reaction (6) it does constitute a valuable endorsement of the internal consistency of the thermodynamic data and of the higher *P* experimental results.

Recalibration of the garnet mixing model

The magnitudes of the free energies of the following four reciprocal reactions strongly affect the garnet activities used in the barometer reaction (1):

$$Ca_3Fe_2Si_3O_{12} + Fe_3Al_2Si_3O_{12} = Fe_3Fe_2Si_3O_{12} + Ca_3Al_2Si_3O_{12} \quad (7)$$

$$Ca_3Fe_2Si_3O_{12} + Mg_3Al_2Si_3O_{12} = Mg_3Fe_2Si_3O_{12} + Ca_3Al_2Si_3O_{12} \quad (8)$$

$$Mg_3Al_2Si_3O_{12} + Ca_3Cr_2Si_3O_{12} = Mg_3Cr_2Si_3O_{12} + Ca_3Al_2Si_3O_{12} \quad (9)$$

$$Fe_3Al_2Si_3O_{12} + Ca_3Cr_2Si_3O_{12} = Fe_3Cr_2Si_3O_{12} + Ca_3Al_2Si_3O_{12}. \quad (10)$$

These four reactions represent the cross-site contributions to the garnet activities (see Appendix), such that $W_{CaAlFeFe3XY} = -\Delta G_{(7)}$, $W_{CaAlMgFe3XY} = -\Delta G_{(8)}$, $W_{CaAlMgCrXY} = -\Delta G_{(9)}$ and $W_{CaAlFeCrXY} = -\Delta G_{(7)}$ are the cross-site energies for garnet X and Y sites (e.g. Powell & Holland, 1993). Gudmundsson & Wood (1995) recognized that varying the garnet mixing parameters, other than for reactions (7) and (8), makes only small differences to results in calculated log f_{O_2} for mantle peridotite garnets with low to moderate Cr contents. Reactions (9) and (10) become significant in Cr-rich garnets. Luth *et al.* (1990) also recognized that $W_{Al,Fe3+} = W_{gr,andr}$ can,

if large in value, lead to significant changes. We find that uncertainties of 10 kJ in these three mixing parameters lead to changes of the order of 0·5 log f_{O_2} units, whereas similar uncertainties on all other mixing parameters produce barely perceptible differences. Although of minor impact, we prefer to include all the within-site mixing energies to avoid any small systematic bias to calculated log f_{O_2}, but concentrate here on the important variables affecting calculated log f_{O_2}.

The thermodynamic dataset of Holland & Powell (2011), updated here with the addition of the skiagite end-member, provides the free energy for reaction (7), $\Delta G_{(7)}$, linearized as $53{\cdot}8 + 0{\cdot}0017T - 0{\cdot}068P$ kJ. Similarly, the free energy of reciprocal reaction (9), $\Delta G_{(7)}$, is given as $10{\cdot}2 - 0{\cdot}0338T + 0{\cdot}121P$ kJ. This last energy is provided by inclusion of uvarovite in the updated Holland & Powell (2011) dataset through the breakdown reaction uvarovite = pseudowollastonite + eskolaite, determined experimentally by Huckenholz & Knittel (1975).

From literature data and the dependent end-member relations (Powell & Holland, 1999) we may derive a complete set of internally consistent garnet mixing energies (see Appendix) involving skiagite and other garnet end-members as follows:

$$W_{py,alm} = 4{\cdot}0 + 0{\cdot}01P \qquad W_{alm,sp} = 2{\cdot}0 + 0{\cdot}02P$$
$$W_{py,gr} = 40{\cdot}0 - 0{\cdot}012T + 0{\cdot}1P \qquad W_{gr,ski} = -47{\cdot}8 - 0{\cdot}0017T + 0{\cdot}168P$$
$$W_{py,ski} = 6{\cdot}0 + 0{\cdot}01P \qquad W_{gr,uv} = 2{\cdot}0$$
$$W_{py,uv} = 31{\cdot}8 + 0{\cdot}0218T - 0{\cdot}021P \qquad W_{gr,sp} = 0{\cdot}06P$$
$$W_{py,sp} = 9{\cdot}0 + 0{\cdot}04P \qquad W_{ski,uv} = -58{\cdot}0 + 0{\cdot}0321T + 0{\cdot}047P$$
$$W_{alm,gr} = 4{\cdot}0 + 0{\cdot}1P \qquad W_{ski,sp} = -19{\cdot}8 - 0{\cdot}0017T + 0{\cdot}058P$$
$$W_{alm,ski} = 2{\cdot}0 \qquad W_{uv,sp} = 32 + 0{\cdot}03P$$
$$W_{alm,uv} = -4{\cdot}2 + 0{\cdot}0338T - 0{\cdot}021P$$

and for a set involving andradite, the following additional energies may be calculated:

$$W_{py,andr} = 95{\cdot}8 - 0{\cdot}0103T + 0{\cdot}032P \qquad W_{gr,andr} = 2{\cdot}0$$
$$W_{alm,andr} = 59{\cdot}8 + 0{\cdot}0017T + 0{\cdot}032P \qquad W_{sp,andr} = 32{\cdot}0 + 0{\cdot}03P$$
$$W_{andr,uv} = 2{\cdot}0 \qquad W_{andr,ski} = 4{\cdot}0 + 0{\cdot}1\mathrm{P}.$$

A new measurement on the entropy (301 J K^{-1}) of knorringite (knor, $Mg_3Cr_2Si_3O_{12}$) has recently been determined by Wijbrans *et al.* (2014) that is slightly smaller than the value (317 J K^{-1}) estimated by Holland & Powell (2011). We have elected to use these updated values in deriving the revised dataset and hence in reaction (9), even though the effects on the oxybarometer are negligibly small (less than 0·01 in log f_{O_2}). It should be noted that, although garnets are asymmetric in their mixing properties (especially for Ca–Mg mixing), a simpler symmetric model has been fitted to garnets that are low in Ca relative to Mg, such as pyropes found in mantle peridotites. Use of the symmetric model has an imperceptible effect on calculated oxygen fugacity.

The equilibrium relation for reaction (1), rewritten as

$$\log f_{O_2} = \frac{1}{\ln(10)}\left(\frac{-\Delta G_{(1)P,T}}{RT} - \ln\frac{a_{fa}^4 a_{fs}}{a_{ski}^2}\right)$$

may be used to determine oxygen fugacity using the expressions in the Appendix for the activities of fa, fs and ski and the free energy of reaction (1).

Revised garnet oxybarometer reactions

The garnet mixing model above may be used directly in reactions such as (1) and (2) to determine oxygen fugacities of garnet-bearing peridotites. With the new thermodynamic data for skiagite it is possible to write 25 barometer reactions among the mineral end-members almandine (alm), skiagite (ski), andradite (andr), grossular (gr), pyrope (py), forsterite (fo), fayalite (fa), enstatite (en), ferrosilite (fs) and oxygen (O_2). However, with 10 end-members and six components (Ca–Mg–Fe–Al–Si–O), only 10 − 6 = 4 of these reactions are independent and provide all the information in the system. We choose the following four independent reactions, using data from the updated Holland & Powell (2011) dataset:

$$2\ \mathrm{ski} = 4\ \mathrm{fa} + \mathrm{fs} + O_2 \qquad (1)$$

$$2\ \mathrm{py} + 2\ \mathrm{andr} + 2\ \mathrm{fs} = 2\,\mathrm{gr} + 4\ \mathrm{fa} + 3\ \mathrm{en} + O_2 \qquad (2)$$

$$2\ \mathrm{ski} + \mathrm{fo} = 5\ \mathrm{fa} + \mathrm{en} + O_2 \qquad (11)$$

$$6\mathrm{ski} + 2\ \mathrm{py} = 2\ \mathrm{alm} + 12\ \mathrm{fa} + 3\ \mathrm{en} + 3O_2 \qquad (12)$$

where reactions (1) and (2) are the equilibria used in the barometers of Gudmundsson & Wood (1995) and Stagno *et al.* (2013), respectively. Both are now formulated on the same set of internally consistent thermodynamic data. It should be noted that reciprocal reaction (7) is one of the 25 reactions that may be written among these end-members and, because it is involved in the garnet mixing model, lends an added degree of internal consistency to the barometry. Each of the four reactions (1), (2), (11) and (12) furnishes a value of log f_{O_2} that will be identical only in the case of perfect activity models, perfect thermodynamic data and perfect equilibrium in the mineral assemblage. However, an optimum log f_{O_2} may be found from these reactions by least squares, analogous to the average pressure calculations of Powell & Holland (1988). In the least squares fit, each reaction carries different weight according to how well its thermodynamic data are known (via uncertainties and correlations among the free energies from the thermodynamic dataset, and in the uncertainties in the mixing parameters for garnet, orthopyroxene and olivine). Additionally, the uncertainties in weight per cent of all oxides in garnet, olivine and orthopyroxene are propagated to contribute to the uncertainty of the activities in each reaction and hence its weight. In these calculations the errors are assigned as follows: in mineral analyses the uncertainty on each oxide weight per cent is taken as 1% relative with a minimum uncertainty of 0·02 wt %. Uncertainty in Fe_2O_3 for garnet is taken as 20% of the measured value [from scatter in experimental measurement and from corrections from 80 K to room temperature (Woodland & Ross, 1994)]. In olivine all Fe is taken

as FeO, and Fe_2O_3 in orthopyroxene is estimated as 0·4 ± 0·3 wt %, based on the 14 tabulated measurements of Canil & O'Neill (1996). These assumptions are much more defensible than estimating Fe_2O_3 from pyroxene stoichiometry, which produces large random variations that may far exceed the measured values of Canil & O'Neill (1996). The uncertainty on each interaction energy (including reciprocal terms) is assigned as 10% relative with a minimum uncertainty of 1·0 kJ, based on typical calorimetric errors, and the uncertainties and correlations between the enthalpies of reaction are taken from the updated Holland & Powell (2011) dataset. Doubling or halving these error assumptions made little difference to calculated log f_{O_2} values. Error propagation is used to determine the covariance matrix ($\boldsymbol{V}$) for the log f_{O_2} values from the four reactions (in column vector $\boldsymbol{F}$) and the optimum f_{av} is found by the least squares result

$$f_{av} = \sigma_{fit}^2(\mathbf{1}^T \boldsymbol{V}^{-1} \boldsymbol{F})$$

where $\sigma_{fit}^2 = (\mathbf{1}^T \boldsymbol{V}^{-1} \mathbf{1})^{-1}$ and $\mathbf{1}$ is a column vector of ones.

The appropriateness of averaging the four reactions in this way is provided by a χ^2 test and the value of σ_{fit}, the mean weighted deviation ($\equiv \sqrt{\text{MSWD}}$). If there is good agreement among the four equilibria within their mutual errors, the overall σ_{fit} is expected to be around 1·0 or less [see the discussion by Powell & Holland (1994) for the analogous case of average pressure calculations]. Values of σ_{fit} significantly greater than a cut-off value of 1·61 [the maximum allowed by a χ^2 test at the 95% confidence level for three degrees of freedom for the four independent reactions; see Powell & Holland (1994)] indicate that the barometers disagree sufficiently and averaging is inappropriate. This could occur either through disequilibrium, through analytical error, or simply by choosing an inappropriate temperature or pressure for the calculation. The correlations among the reactions frequently cause the calculated optimal log f_{O_2} to differ considerably from a simple average of the four log f_{O_2} values. Enlarging the assumed uncertainties on the input variables (e.g. chemical analyses, W values, etc.) will cause σ_{fit} to be smaller, so a failure of the χ^2 test may be flagging that input uncertainties have been underestimated rather than pointing to disequilibrium in the sample.

Output is shown in Table 2 from program *GtfO2* for a mantle garnet-harzburgite from the Finsch mine, Kaapvaal Craton (F5; Lazarov *et al.*, 2009) that equilibrated at 54 kbar and 1150°C (Table 3). The output shows input mineral analyses for garnet, orthopyroxene and olivine, recalculated cations and their uncertainties, and calculated activities for end-members used in oxybarometry. The calculated Δlog f_{O_2} (FMQ) values are –2·69 ± 0·89, –2·40 ± 0·90, –2·45 ± 0·88 and –1·95 ± 0·90 for reactions (1), (2), (11) and (12), respectively. The least squares optimum is –2·63 ± 1·28, with a σ_{fit} value (labelled f in the output) of 1·49. This is smaller than the cut-off of 1·61 so combining the reactions is appropriate and the assemblage is reasonably well equilibrated. The fact that the χ^2 test for internal consistency among the four independent reactions is passed

Table 2. Example output from program GtfO2; sample F5, for P = 54·4 kbar and T = 1150°C

	SiO_2	TiO_2	Al_2O_3	Cr_2O_3	Fe_2O_3	FeO	MnO	MgO	CaO	Na_2O	K_2O	Total
Garnet												
wt %	42·27	0·08	19·03	6·36	0·41	5·98	0·32	21·08	5·75	0·02	0·00	101·30
cations	2·998	0·004	1·591	0·357	0·022	0·355	0·019	2·228	0·437	0·003	0·000	8·014
cat ±	0·028	0·001	0·025	0·007	0·015	0·017	0·001	0·035	0·009	0·003	0·000	
ln *a*(py) = –1·18 (± 0·03)												
ln *a*(al) = –6·69 (± 0·13)												
ln *a*(sk) = –15·78 (± 1·37)												
Orthopyroxene												
wt %	58·53	0·01	0·56	0·30	0·40	4·07	0·11	36·40	0·64	0·09	0·00	101·11
cations	1·980	0·000	0·022	0·008	0·010	0·115	0·003	1·835	0·023	0·006	0·000	4·003
cat ±	0·014	0·001	0·001	0·001	0·005	0·006	0·001	0·027	0·001	0·001	0·000	
ln *a*(fs) = –5·38 (± 0·10)												
ln *a*(en) = –0·17 (± 0·03)												
Olivine												
wt %	41·48	0·00	0·00	0·00	0·00	7·06	0·09	51·08	0·03	0·00	0·00	99·74
cations	1·005	0·000	0·000	0·000	0·000	0·143	0·002	1·844	0·001	0·000	0·000	2·995
cat ±	0·011	0·000	0·000	0·000	0·000	0·003	0·000	0·021	0·001	0·000	0·000	
ln *a*(fa) = –4·74 (± 0·04)												
ln *a*(fo) = –0·16 (± 0·02)												

Reaction	log f_{O_2}	±	DelFMQ	
FMQ	–5·40	0·06		$2mt + 3q = 3fa + 2O_2$
R1	–8·09	0·89	–2·69	$2ski = 4fa + fs + O_2$
R2	–7·80	0·90	–2·40	$2ski + fo = 5fa + en + O_2$
R3	–7·85	0·88	–2·45	$6ski + 2py = 2alm + 12fa + 3en + 3O_2$
R4	–7·35	0·90	–1·95	$2py + 2andr + 2fs = 2gr + 4fa + 3en + O_2$
avfo2	–8·03	1·28	–2·63	with f = 1·49 (limit 1·61)

Table 3. Pressure, temperature and oxygen fugacity estimates for mantle xenoliths from the Baikal Rift, Siberian Craton, Kaapvaal Craton, and Slave Craton

Sample	Rock type	This study				Published data			
				$\Delta\log f_{O_2}$ (FMQ)				$\Delta\log f_{O_2}$ (FMQ)	
		P (kbar)	*T* (°C)	Sp	Gt	*P* (kbar)	*T* (°C)	Sp (BW90)	Gt (GW95)
Baikal Rift, Vitim Field									
Spinel lherzolites									
314-56	lherz	16·7	858	–0·84	n.a.	15·0	818	–0·77	n.a.
314-58	lherz	15·8	813	–0·44	n.a.	14·0	775	–0·29	n.a.
Vt11	lherz	17·2	881	0·54	n.a.	17·0	937	0·62	n.a.
Vt12	lherz	16·4	850	–0·22	n.a.	16·0	885	–0·19	n.a.
314-5	lherz	20·8	1048	–0·05	n.a.	21·0	1055	0·28	n.a.
314-6	lherz	21·1	1072	–1·29	n.a.	19·0	1006	–0·96	n.a.
314-59	lherz	21·9	1101	–0·79	n.a.	21·0	1061	–0·24	n.a.
Vt13	lherz	22·0	1105	0·01	n.a.	22·0	1109	0·65	n.a.
Vt14	lherz	21·0	1066	–0·67	n.a.	22·0	1098	–0·32	n.a.
Garnet–spinel lherzolites									
313-5	lherz	21·4	1087	–0·35	–1·79	22·0	1097	0·11	–2·97
313-37	lherz	22·9	1074	–0·38	n.a.	22·0	1031	–0·09	n.a.
314-74	lherz	20·6	1067	–0·03	n.a.	23·0	1103	–0·09	n.a.
314-230	lherz	20·6	1074	–0·43	n.a.	21·0	1077	–0·07	n.a.
314-580	lherz	22·0	1106	–0·17	n.a.	22·0	1096	–0·07	n.a.
Vt4	lherz	19·4	1044	0·20	–0·78	20·0	1065	0·30	–2·10
Vt6	lherz	19·7	1012	n.a.	–1·59	21·0	1030	n.a.	–3·02
Vt7	lherz	20·9	1073	–0·32	–1·58	22·0	1092	–0·01	–3·16
Vt8	lherz	20·4	1069	–0·25	–1·16	21·0	1089	–0·41	–2·62
Vt9	lherz	22·0	1057	0·11	–1·52	24·0	1096	0·26	–2·84
Vt15	lherz	18·3	929	–0·09	–0·14	21·0	985	–0·09	–1·60
Vt37	lherz	20·5	1041	n.a.	–0·56	21·0	1053	n.a.	–1·87
Vt44	lherz	20·0	1018	n.a.	–0·98	21·0	1031	n.a.	–2·34
Vt52	lherz	21·2	1074	n.a.	–0·67	22·0	1099	n.a.	–1·97
Garnet lherzolites									
313-3	lherz	21·9	1023	n.a.	–1·82	21·0	981	n.a.	–2·84
313-4	lherz	20·7	1032	n.a.	–1·81	20·0	1027	n.a.	–2·93
313-6	lherz	20·5	1041	n.a.	–1·80	21·0	1053	n.a.	–2·86
313-8	lherz	21·6	1067	n.a.	–1·67	21·0	1039	n.a.	–2·81
Vt5	lherz	20·0	1037	n.a.	–0·92	21·0	1053	n.a.	–2·50
Vt16	lherz	19·9	1040	n.a.	–1·11	20·0	1051	n.a.	–2·53
Vt19	lherz	22·0	1040	n.a.	–0·41	24·0	1078	n.a.	–1·98
Vt20	lherz	20·8	1031	n.a.	–0·58	23·0	1076	n.a.	–1·96
Vt39	lherz	20·3	1034	n.a.	–1·52	21·0	1045	n.a.	–2·89
Vt40	lherz	20·0	1030	n.a.	–1·11	20·0	1041	n.a.	–2·51
Vt43	lherz	22·9	1173	n.a.	–1·47	25·0	1186	n.a.	–2·79
Vt46	lherz	20·2	1024	n.a.	–1·58	21·0	1036	n.a.	–2·82
Vt47	lherz	19·1	989	n.a.	–1·53	20·0	1005	n.a.	–2·93
Siberian Craton, Udachnaya									
Spinel-bearing peridotites									
U15	harz	33·3	827	–0·60	n.a.	38·0	917	0·02	n.a.
U24	harz	28·4	742	–1·09	n.a.	29·0	763	–0·65	n.a.
U52	harz	24·6	678	–0·55	n.a.	27·0	738	–0·20	n.a.
U97	harz	23·9	667	–0·09	n.a.	24·0	676	0·76	n.a.
U151	lherz	32·2	806	–0·52	n.a.	25·0	692	0·62	n.a.
U504	harz	30·5	779	–1·71	n.a.	29·0	761	–0·93	n.a.
U1123	harz	22·5	779	–0·36	n.a.	21·0	615	0·31	n.a.
87/55	harz	32·7	815	n.a.	n.a.	32·0	811	n.a.	n.a.
87/72	dun	32·9	818	n.a.	n.a.	32·0	814	n.a.	n.a.
Garnet–spinel harzburgites									
U283	harz	29·3	762	–1·37	0·23	32·0	791	–1·01	–0·88
87/100	harz	46·2	1132	n.a.	–2·66	46·0	1132	n.a.	–2·43
87/59	harz	42·0	552	n.a.	–2·06	42·0	950	n.a.	–4·64
Garnet-bearing peridotites									
Uv-4-05	lherz	62·3	1292	n.a.	–2·03	62·3	1292	n.a.	–3·70
Uv-9-05	lherz	30·9	768	n.a.	–1·08	31·0	770	n.a.	–2·50
Uv-26-04	lherz	51·5	960	n.a.	–1·81	51·6	962	n.a.	–3·40
Uv-50-04	lherz	56·1	1278	n.a.	–3·60	56·1	1278	n.a.	–5·00
Uv-129-03	lherz	53·4	1167	n.a.	–1·34	53·5	1168	n.a.	–3·30
Uv-87-03	lherz	61·2	1324	n.a.	–1·86	61·2	1324	n.a.	–3·60
Uv-59-03	lherz	59·3	1244	n.a.	–2·31	59·3	1244	n.a.	–4·00
Uv-45-03	lherz	36·9	897	n.a.	–1·88	37·0	899	n.a.	–3·00

(continued)

Table 3. Continued

Sample	Rock type	This study				Published data			
				$\Delta\log f_{O_2}$ (FMQ)				$\Delta\log f_{O_2}$ (FMQ)	
		P (kbar)	*T* (°C)	Sp	Gt	*P* (kbar)	*T* (°C)	Sp (BW90)	Gt (GW95)
Uv-88-03	lherz	69·0	1363	n.a.	−2·39	69·0	1364	n.a.	−4·00
Uv-130-03	lherz	70·6	1259	n.a.	−4·93	70·6	1259	n.a.	−5·90
Uv-68-03	lherz	52·6	1234	n.a.	−1·93	52·7	1234	n.a.	−3·60
Uv-89-03	lherz	64·3	1252	n.a.	−2·58	64·4	1253	n.a.	−4·30
Uv-34-03	lherz	61·3	1289	n.a.	−1·58	61·3	1290	n.a.	−3·40
Uv-42-03	lherz	38·7	945	n.a.	−2·67	38·8	947	n.a.	−4·00
U29	lherz	48·3	911	n.a.	−2·00	50·0	897	n.a.	−3·27
U64	harz	56·2	1194	n.a.	−2·32	61·0	1211	n.a.	−3·36
U501	harz	48·9	895	n.a.	−2·27	47·0	859	n.a.	−3·28
U506	harz	59·1	988	n.a.	−1·92	55·0	941	n.a.	−3·03
Y17	lherz	29·0	781	n.a.	−1·24	29·0	784	n.a.	−3·49
U4	lherz	59·0	1305	n.a.	−1·66	59·0	1308	n.a.	−2·96
U9	harz	51·9	1170	n.a.	−1·40	57·0	1239	n.a.	−2·67
U10	harz	61·6	1293	n.a.	−2·02	63·0	1295	n.a.	−3·05
U50	lherz	56·9	1271	n.a.	−1·46	60·0	1287	n.a.	−3·00
U70	lherz	51·4	1233	n.a.	−1·46	63·0	1268	n.a.	−3·52
U71	harz	58·4	1266	n.a.	−1·80	63·0	1293	n.a.	−3·24
U85	lherz	53·1	1216	n.a.	−2·08	55·0	1240	n.a.	−3·57
U148	lherz	58·3	1261	n.a.	−2·19	60·0	1274	n.a.	−3·61
U183	harz	64·0	1224	n.a.	−2·99	64·0	1241	n.a.	−3·76
U267	lherz	58·8	1257	n.a.	−2·45	54·0	1221	n.a.	−3·58
U507	lherz	59·6	1284	n.a.	−2·37	60·0	1290	n.a.	−3·87
87/114	harz	51·9	1247	n.a.	−1·02	52·0	1248	n.a.	−1·91
87/70	harz	54·3	1231	n.a.	−1·63	54·0	1232	n.a.	−2·53
87/97	lherz	56·5	1350	n.a.	−2·67	57·0	1350	n.a.	−4·02
Y1	lherz	52·1	1242	n.a.	−1·27	52·0	1243	n.a.	−1·80
Y3	lherz	53·0	1238	n.a.	−2·17	53·0	1238	n.a.	−3·72
Y4	lherz	50·4	1225	n.a.	−1·05	50·0	1225	n.a.	−1·98
Y10	lherz	51·3	1163	n.a.	−1·95	51·0	1163	n.a.	−2·90
Y16	wehr	52·0	1250	n.a.	−1·60	52·0	1251	n.a.	−2·91
Y19	wehr	45·9	1181	n.a.	−1·41	46·0	1181	n.a.	−2·42
Kaapvaal Craton, Finsch									
Garnet-bearing peridotites									
F1	harz	51·1	1153	n.a.	−1·87	57·0	1204	n.a.	−3·76
F2	dun	55·5	1190	n.a.	−2·59	47·0	1066	n.a.	−3·17
F3	dun	52·4	1125	n.a.	−2·35	48·0	1178	n.a.	−3·16
F5	harz	54·4	1150	n.a.	−2·63	50·0	1149	n.a.	−3·67
F6	harz	53·2	1181	n.a.	−2·34	53·0	1203	n.a.	−3·58
F7	harz	60·3	1222	n.a.	−3·12	49·0	1109	n.a.	−3·65
F8	dun	55·5	1166	n.a.	−2·57	56·0	1189	n.a.	−3·70
F9	harz	55·9	1156	n.a.	−2·46	48·0	1073	n.a.	−2·53
F11	harz	54·3	1187	n.a.	−2·38	53·0	1224	n.a.	−4·06
F12	harz	56·8	1134	n.a.	−2·64	59·0	1197	n.a.	−3·81
F14	harz	59·3	1208	n.a.	−2·60	57·0	1179	n.a.	−3·67
F15	lherz	52·5	1157	n.a.	−2·49	55·0	1193	n.a.	−3·92
F16	lherz	50·8	1156	n.a.	−2·44	59·0	1207	n.a.	−4·64
556-XM48	harz	58·9	1220	n.a.	−2·68	54·0	1191	n.a.	n.a.
695	55·9	1172	n.a.	−2·77	56·0	1196	n.a.	−3·46	
865	harz	64·0	1282	n.a.	−3·78	59·0	1161	n.a.	−4·71
Kaapvaal Craton, other Kaapvaal									
Spinel-bearing harzburgites									
Let 19	harz	n.a.	n.a.	−0·88	n.a.	25·0	986	−0·67	n.a.
Let 23	harz	n.a.	n.a.	−0·05	n.a.	25·0	901	−0·11	n.a.
Liq 9	harz	n.a.	n.a.	−1·12	n.a.	30·0	920	−0·91	n.a.
Kim 8	harz	n.a.	n.a.	0·29	n.a.	46·0	997	0·94	n.a.
Garnet-bearing peridotites									
Let 1	lherz	n.a.	n.a.	n.a.	−2·47	45·0	1113	n.a.	−3·30
Let 4	harz	n.a.	n.a.	n.a.	−2·27	40·5	993	n.a.	−3·31
Let 6	lherz	n.a.	n.a.	n.a.	−1·10	34·3	928	n.a.	−2·31
Let 7	lherz	n.a.	n.a.	n.a.	−1·81	37·2	912	n.a.	−2·49
Let 8	sheared	n.a.	n.a.	n.a.	−2·45	48·6	1177	n.a.	−3·28
Let 9	sheared	n.a.	n.a.	n.a.	−2·79	63·6	1429	n.a.	−4·12
Let 12	sheared	n.a.	n.a.	n.a.	−2·32	62·0	1389	n.a.	−3·63
Let 14	lherz	n.a.	n.a.	n.a.	−2·18	44·5	1108	n.a.	−3·31
Let 21	lherz	n.a.	n.a.	n.a.	−2·35	44·2	1029	n.a.	−3·30

(continued)

Table 3. Continued

Sample	Rock type	This study				Published data			
				Δlog f_{O_2} (FMQ)				Δlog f_{O_2} (FMQ)	
		P (kbar)	*T* (°C)	Sp	Gt	*P* (kbar)	*T* (°C)	Sp (BW90)	Gt (GW95)
Let 22	lherz	n.a.	n.a.	n.a.	–2·26	43·5	1066	n.a.	–3·17
Let 39	lherz	n.a.	n.a.	n.a.	–2·39	46·4	1083	n.a.	–3·37
Liq 1	lherz	n.a.	n.a.	n.a.	–2·33	46·3	1157	n.a.	–3·18
Liq 5	harz	n.a.	n.a.	n.a.	–2·94	45·2	1079	n.a.	–3·91
Liq 10	harz	n.a.	n.a.	n.a.	–1·35	38·0	1010	n.a.	–2·46
Liq 11	lherz	n.a.	n.a.	n.a.	–2·45	44·7	1083	n.a.	–3·45
Mat 2	lherz	n.a.	n.a.	n.a.	–2·15	42·1	1042	n.a.	–3·16
Mat 4	lherz	n.a.	n.a.	n.a.	–2·49	45·5	1106	n.a.	–3·39
Mat 5	lherz	n.a.	n.a.	n.a.	–2·20	41·4	1049	n.a.	–3·30
Mat 7	lherz	n.a.	n.a.	n.a.	–2·41	42·5	1028	n.a.	–3·12
Mat 10	lherz	n.a.	n.a.	n.a.	–2·19	42·5	1055	n.a.	–3·33
Mat 12	lherz	n.a.	n.a.	n.a.	–2·53	44·0	1077	n.a.	–3·46
Mat 13	lherz	n.a.	n.a.	n.a.	–2·44	45·7	1069	n.a.	–3·46
Jag 1	lherz	n.a.	n.a.	n.a.	–2·78	62·0	1353	n.a.	–4·14
Jag 2	lherz	n.a.	n.a.	n.a.	–1·68	45·0	1098	n.a.	–3·08
Jag 4	sheared	n.a.	n.a.	n.a.	–2·21	52·7	1337	n.a.	–3·21
Jag 7	sheared	n.a.	n.a.	n.a.	–2·76	60·4	1290	n.a.	–4·12
Jag 9	harz	n.a.	n.a.	n.a.	–2·58	55·0	1259	n.a.	–3·87
Mon 2	lherz	n.a.	n.a.	n.a.	–1·58	37·9	935	n.a.	–2·64
Mon 5	harz	n.a.	n.a.	n.a.	–2·16	41·0	1011	n.a.	–3·28
FSM 1	lherz	n.a.	n.a.	n.a.	–2·71	60·0	1355	n.a.	–3·99
Kim 1	lherz	n.a.	n.a.	n.a.	–1·96	43·7	1112	n.a.	–2·81
Kim 5	harz	n.a.	n.a.	n.a.	–1·92	42·6	1082	n.a.	–3·13
Kim 11	harz	n.a.	n.a.	n.a.	–1·91	42·1	1071	n.a.	–2·88
Kim 13	lherz	n.a.	n.a.	n.a.	–2·58	53·5	1198	n.a.	–3·47
Kim 14a	harz	n.a.	n.a.	n.a.	–1·51	42·3	1037	n.a.	–2·58
Kim 17	harz	n.a.	n.a.	n.a.	–1·92	46·4	1196	n.a.	–2·62
Kim 22	harz	n.a.	n.a.	n.a.	–0·98	33·7	894	n.a.	–1·98
Kim 24	harz	n.a.	n.a.	n.a.	–0·67	35·7	952	n.a.	–1·81
Kim 25	lherz	n.a.	n.a.	n.a.	–1·90	43·0	1048	n.a.	–2·99
Kim 30	lherz	n.a.	n.a.	n.a.	–1·94	43·1	1020	n.a.	–3·01
Kim 35	lherz	n.a.	n.a.	n.a.	–1·23	39·8	1016	n.a.	–2·52
Kim 38	lherz	n.a.	n.a.	n.a.	–1·90	44·6	1081	n.a.	–2·91
Kim 44	lherz	n.a.	n.a.	n.a.	–1·47	41·7	1091	n.a.	–2·20
Kim 45	lherz	n.a.	n.a.	n.a.	–1·63	42·1	1043	n.a.	–2·66
Kim 48	lherz	n.a.	n.a.	n.a.	–2·36	46·4	1117	n.a.	–3·25
KBD7	lherz	45·0	1086	n.a.	–2·74	40·9	1008	n.a.	–3·33
KBD12(c)	lherz	43·3	1042	n.a.	–1·59	47·4	1116	n.a.	–2·43
KBD12(r)	lherz	43·7	1040	n.a.	–0·57	46·1	1124	n.a.	–1·02
KBD18	lherz	38·8	938	n.a.	–0·90	35·8	887	n.a.	–1·70
Wesselton(c)	lherz	50·6	1061	n.a.	–1·68	47·0	1060	n.a.	–3·00
Wesselton(r)	lherz	50·0	1059	n.a.	–0·61	47·0	1060	n.a.	–1·20
Slave Craton, Diavik Mine									
Spinel-bearing peridotites									
8-7	lherz	30·0	696	–1·71	n.a.	25	683	–1·3	n.a.
44-12	lherz	34·2	770	–2·44	n.a.	30	771	–1·8	n.a.
Garnet–spinel peridotites									
10-12a	lherz	33·2	744	0·17	–1·20	30·3	792	0·4	–1·8
21-1	lherz	32·1	783	0·44	–1·10	30·8	811	0·4	–2·9
26-11	lherz	43·2	926	0·13	–1·44	42·7	944	0·6	–2·1
Garnet-bearing peridotites									
A154-01	lherz	60·5	1181	n.a.	–2·91	67·9	1227	n.a.	–3·71
A154-06	lherz	56·4	1195	n.a.	–0·53	53·9	1176	n.a.	–1·70
A154-09CR	lherz	50·8	1092	n.a.	–1·39	54·0	1146	n.a.	–2·84
A154-10	harz	55·4	1145	n.a.	–0·44	44·7	1032	n.a.	–1·01
MX001	lherz	56·8	1260	n.a.	–1·18	57·3	1293	n.a.	–2·46
MX029	lherz	59·6	1190	n.a.	–0·82	68·0	1246	n.a.	–2·13
MX031	harz	54·3	1140	n.a.	–0·83	44·4	1045	n.a.	–1·28
MX032	lherz	60·6	1239	n.a.	–0·35	57·1	1239	n.a.	–1·67
MX044	lherz	59·1	1299	n.a.	–0·47	66·0	1346	n.a.	–2·70
MX088	lherz	57·5	1174	n.a.	–0·68	60·0	1206	n.a.	–2·44
MX104	lherz	62·6	1255	n.a.	–2·82	68·4	1293	n.a.	–4·31
MX118	harz	60·2	1225	n.a.	–1·43	49·9	1110	n.a.	–2·00
MX131	lherz	55·6	1232	n.a.	–2·17	62·8	1282	n.a.	–3·92
MX144	lherz	55·1	1214	n.a.	–1·70	64·5	1281	n.a.	–3·81

(continued)

Table 3. Continued

Sample	Rock type	This study				Published data			
				Δlog f_{O_2} (FMQ)				Δlog f_{O_2} (FMQ)	
		P (kbar)	*T* (°C)	Sp	Gt	*P* (kbar)	*T* (°C)	Sp (BW90)	Gt (GW95)
MX158	lherz	62·0	1174	n.a.	−2·57	68·0	1200	n.a.	−4·27
MX162	lherz	56·3	1196	n.a.	−1·98	58·6	1244	n.a.	−3·35
MX165	lherz	62·0	1245	n.a.	−1·38	61·9	1257	n.a.	−2·58
MX5000	lherz	60·4	1259	n.a.	−2·83	63·1	1261	n.a.	−4·23
MX5001	lherz	58·4	1235	n.a.	−1·38	61·9	1241	n.a.	−3·05
MX5003	lherz	43·0	903	n.a.	0·03	40·5	913	n.a.	−0·71
MX5004	lherz	57·0	1211	n.a.	−1·64	57·6	1223	n.a.	−2·90
MX5006	lherz	58·6	1212	n.a.	−1·82	59·1	1237	n.a.	−3·01
MX5007	harz	41·8	875	n.a.	−1·03	25·7	777	n.a.	−0·58
MX5008	lherz	60·6	1256	n.a.	−1·25	68·5	1304	n.a.	−3·29
MX5009	lherz	59·9	1275	n.a.	−1·43	62·7	1316	n.a.	−2·91
MX5010	harz	44·4	857	n.a.	−0·61	27·6	714	n.a.	0·15
MX5011	lherz	58·7	1261	n.a.	−3·21	57·0	1271	n.a.	−3·95
MX5012	lherz	52·7	1189	n.a.	−2·23	56·0	1238	n.a.	−3·58
MX5020	harz	58·5	1236	n.a.	−1·43	52·8	1135	n.a.	−2·40
22-5	lherz	40·4	861	n.a.	−1·02	42·9	951	n.a.	−2·2
25-4	lherz	48·0	980	n.a.	−2·14	47·7	975	n.a.	−2·6
25-9	lherz	34·2	769	n.a.	−1·49	36·6	842	n.a.	−3·1
14-107	lherz	47·8	992	n.a.	−0·18	51·6	1068	n.a.	−1·9
40-11	lherz	49·0	1037	n.a.	−2·13	52·1	1104	n.a.	−3·4
21-6	lherz	55·5	1121	n.a.	−2·51	62·2	1190	n.a.	−4·2
21-4	lherz	47·0	1003	n.a.	−1·96	55·2	1097	n.a.	−3·8
21-3	lherz	84·9	1121	n.a.	−4·91	51·2	1088	n.a.	−3·7
22-7	lherz	84·2	1205	n.a.	−3·94	53·4	1187	n.a.	−2·9
41-1	lherz	51·0	1197	n.a.	−1·00	55·5	1274	n.a.	−2·4
8-1	lherz	53·1	1216	n.a.	−2·38	56·4	1282	n.a.	−3·5
14-78	lherz	78·1	1303	n.a.	−4·52	59	1300	n.a.	−4·2
40-38	lherz	54·1	1265	n.a.	−1·55	49·5	1286	n.a.	−2·0
23-5	lherz	50·8	1189	n.a.	−1·39	59·2	1262	n.a.	−3·2
9-10	lherz	53·7	1129	n.a.	−1·76	62·9	1214	n.a.	−3·5
14-124	lherz	55·7	1155	n.a.	−2·06	64·2	1230	n.a.	−3·8
41-3	lherz	50·0	1188	n.a.	−1·15	60	1281	n.a.	−3·1
32-2	lherz	53·3	1083	n.a.	−1·52	68·3	1178	n.a.	−4·1
99-12	lherz	66·2	1167	n.a.	−3·73	56·5	1026	n.a.	−4·2
18-1	lherz	51·8	1046	n.a.	−1·96	61·7	1139	n.a.	−3·8
38-2	lherz	45·6	872	n.a.	−2·34	49·1	971	n.a.	−3·9
11-5	lherz	61·0	1174	n.a.	−2·50	64·8	1255	n.a.	−3·6
99-14C	lherz	53·8	1064	n.a.	−1·87	52·3	1027	n.a.	−3·1
38-1	lherz	55·2	1066	n.a.	−2·61	62·3	1122	n.a.	−4·2

Rock types: lherz, lherzolite; harz, harzburgite; dun, dunite; wehr, wehrlite; sheared, sheared lherzolite. Data sources for Baikal Rift: Ionov *et al.* (2005) and Goncharov & Ionov (2012). Data sources for Siberian Craton: Ionov *et al.* (2010), Goncharov *et al.* (2012) and Yaxley *et al.* (2012). Data sources for Kaapvaal Craton: Woodland & Koch (2003), Lazarov *et al.* (2009), Berry *et al.* (2013) and Hanger *et al.* (2015). Data sources for Slave Craton: Kopylova *et al.* (1999), Kopylova & Caro (2004), McCammon & Kopylova (2004) and Creighton *et al.* (2009). n.a., not applicable.

in the majority of natural samples investigated here confirms the internal consistency now attainable between the skiagite barometer (1) and the andradite barometer (2).

Typical uncertainties for each barometer reaction lie in the range 0·6–0·9 log f_{O_2} units, depending mainly on mineral compositional uncertainties, particularly in ferric iron content. If all reactions agree within mutual error then the overall uncertainty will be of this magnitude. However, if the barometers do not mutually agree then σ_{fit} will be greater than 1·0 and the overall error will be enlarged through multiplication by σ_{fit}. Thus the minimum uncertainty on log f_{O_2} will be of the order of 0·6–0·9 log units.

Figure 2a illustrates the experimental log f_{O_2} data from Gudmundsson & Wood (1995) and Stagno *et al.* (2013) compared with calculations from reactions (1) and (2). Calculated values tend to be somewhat scattered, but with uncertainties on calculated and experimental values being of the order of 2 and 1 log units, respectively, the agreement is deemed satisfactory. The calculated results tend to be higher at more reducing conditions but are in fairly good agreement at higher log f_{O_2}, perhaps more so with the experiments of Stagno *et al.* (2013). It should be noted that only about 20% of the experimental samples of Gudmundsson & Wood (1995) and Stagno *et al.* (2013) pass the χ^2 test, suggesting that the experimental runs may not have fully equilibrated. This should not be surprising, however, as experiments of short duration are likely to be less well equilibrated than natural samples. When the least squares results using all four equilibria (1), (2), (11)

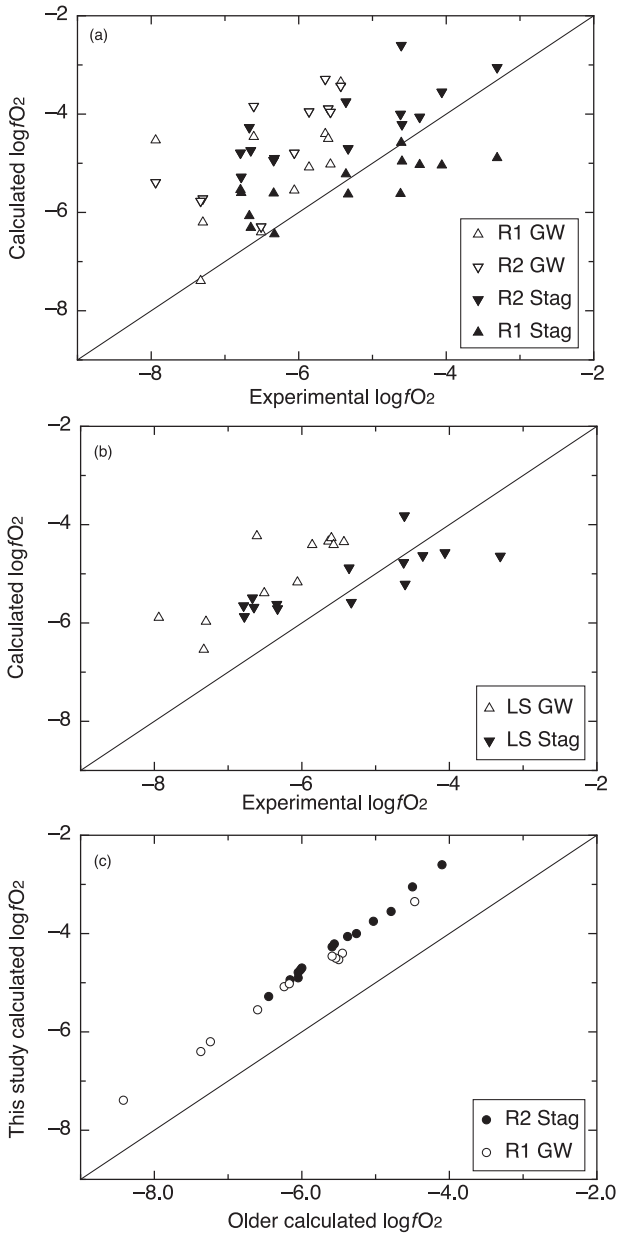

Fig. 2. Calculated log f_{O_2} compared with experiments. (a) The experiments of Gudmundsson & Wood (1995) (GW) and of Stagno *et al.* (2013) (Stag). Upward-facing triangles are for reaction (1) and downward-facing triangles are for reaction (2). (b) The same data but for the least squares calculation using reactions (1), (2), (11) and (12). The least squares results are less scattered than those for each of the barometers and in better agreement with the experiments. (c) Comparison of calculations using the new calibrations against the original result of Gudmundsson & Wood (1995) (GW) and that of Stagno *et al.* (2013) (Stag); this shows a consistent 1–1·5 log unit offset.

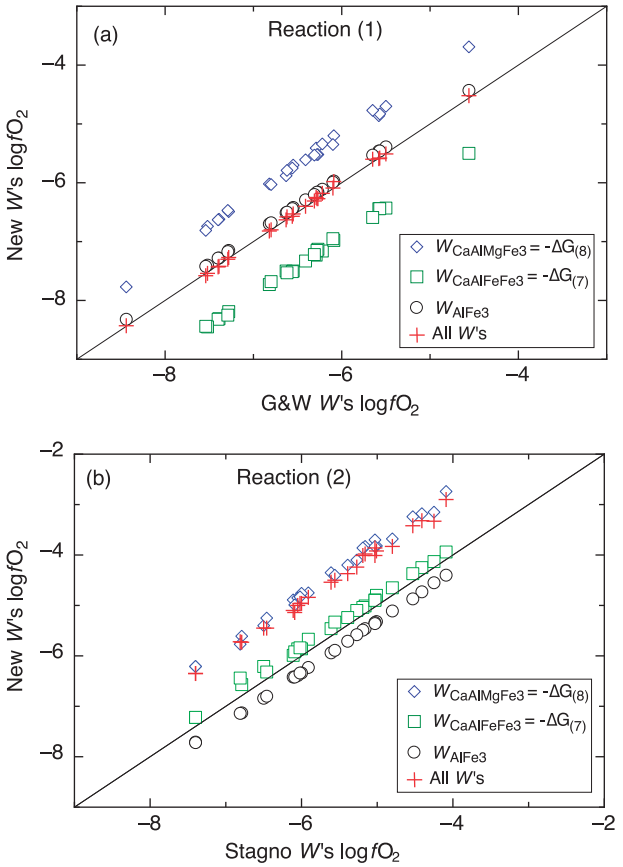

Fig. 3. The effect on calculated log f_{O_2} of varying three significant garnet W mixing parameters. (a) The calculations on reaction (1) using the calibration of Gudmundsson & Wood (1995) on the x-axis and similar calculations varying W parameters on the y-axis. Circles, W_{AlFe3+} changed to 2·0 kJ; diamonds, $W_{CaAlMgFe3XY}$ changed by +23 kJ; squares, $W_{CaAlFeFe3XY}$ changed by +23 kJ; crosses, all three changes. (b) The equivalent calculations on reaction (2) using the calibration of Stagno *et al.* (2013). Symbols as for (a). [Note the cumulative effects of $W_{CaAlMgFe3XY}$ and $W_{CaAlFeFe3XY}$ for reaction (2) as opposed to the compensating effects in reaction (1).]

and (12) are compared with the experiments (Fig. 2b) the results are less scattered, illustrating the more robust estimation of log f_{O_2} values in comparison with those from each of the equilibria. Figure 2c is a plot of the new calibration expressions for reactions (1) and (2) against the original barometer expressions of Gudmundsson & Wood (1995) and Stagno *et al.* (2013) and shows the fairly uniform relative offset of 1–1·5 log units of the new calibrations. Given that Stagno *et al.* (2013) used the Holland & Powell (2011) dataset, the offset relative to their expression must be caused by the different interaction energies in garnet, especially in the two reciprocal reactions (7) and (8) and the large value of $W_{Al,Fe3+}$ used by them. The differences between the new calibrations and earlier studies for reactions (1) and (2) may be seen readily in Fig. 3. In Fig. 3a the separate effects of replacing the interaction energies ($W_{CaAlFeFe3XY} = -\Delta G_{(7)}$, $W_{CaAlMgFe3XY} = -\Delta G_{(8)}$ and $W_{Al,Fe3+}$) used by Gudmundsson & Wood (1995) by the new ones used in this study are illustrated clearly. Changing $W_{Al,Fe3+}$ from zero to 2·0 kJ has only a small impact whereas the other two have large and opposite effects on log f_{O_2}. The opposing effects mean that changing $W_{CaAlFeFe3XY}$ and $W_{CaAlMgFe3XY}$ by the same amount (23 kJ) has only a negligible effect on log f_{O_2}. The net effect of changing all three Ws together gives a result fortuitously identical to the original

Gudmundsson & Wood (1995) expression, and thus demonstrates that the difference between our new calibration and the original barometer lies entirely with the revised Gibbs energy for reaction (1). Figure 3b shows a rather different situation for reaction (2) where the effects of $W_{CaAlFeFe3XY}$ and $W_{Al,Fe3+}$ are small but that of $W_{CaAlMgFe3XY}$ is large. In contrast to reaction (1) changes of 23 kJ in both $W_{CaAlFeFe3XY}$ and $W_{CaAlMgFe3XY}$ move log f_{O_2} in the same direction. Changing all three Ws simultaneously to the new values raises log f_{O_2} by around 1 log unit and it is these W differences and not any change in Gibbs energy of reaction (2) that make our new calibration differ from that of Stagno *et al.* (2013). The internal inconsistency in the Stagno *et al.* (2013) barometer lies in their values for $W_{CaAlFeFe3XY}$ and $W_{CaAlMgFe3XY}$, which do not agree with the free energies in the updated Holland & Powell (2011) dataset (Table 1) for reactions (7) and (8). Making both $W_{CaAlFeFe3XY}$ and $W_{CaAlMgFe3XY}$ larger barely affects reaction (1) because of the opposing senses of change, whereas reaction (2) is additively affected. Reaction (1) was well chosen by Gudmundsson & Wood (1995) in being more robust to uncertainties in mixing parameters.

The new barometer results are in fairly close agreement with the experimental data of Stagno *et al.* (2013) as shown in Fig. 2b. The lack of perfect agreement of the new calibrations with the high-pressure metal sensor techniques (Gudmundsson & Wood, 1995; Stagno *et al.*, 2013) will be discussed after reassessment of the spinel oxybarometer.

REVISED SPINEL OXYBAROMETER EQUILIBRIA

The advantage of solving several reactions simultaneously by the least squares method makes it desirable to extend this approach to spinel oxybarometry. The following three independent equilibria are used:

$$2\ \mathrm{mt} + 3\ \mathrm{fs} = 6\ \mathrm{fa} + \mathrm{O_2} \quad (13)$$

$$2\ \mathrm{mt} + 3\ \mathrm{en} = 3\ \mathrm{fa} + 3\ \mathrm{fo} + \mathrm{O_2} \quad (14)$$

$$2\ \mathrm{mt} + 3\ \mathrm{en} + 6\ \mathrm{hc} = 6\ \mathrm{sp} + 6\ \mathrm{fa} + \mathrm{O_2}. \quad (15)$$

The first of these three equilibria was calibrated by Bryndzia & Wood (1990) and has been used widely since. We use the activity model for spinel from Bryndzia & Wood (1990) coupled with thermodynamic data from Holland & Powell (2011). The free energies for (13) are virtually indistinguishable from those given by Bryndzia & Wood (1990). It is important to note that (13) is rather sensitive to the activity of fs. This is significant because the mol fraction of fs in mantle orthopyroxenes is very small and poorly determined (especially with uncertain Fe_2O_3 content) and because the earlier calibrations assumed ideal mixing. Reaction (14) is more resistant to uncertainty as (1) it does not depend on the fs end-member, (2) it involves fo and en end-members, which have large and better determined activities in olivine and opx, and (3) the Mg-poor silicate end-member is fa, the activity of which is more reliably estimated than that of fs. When averaging log f_{O_2} from (13), (14) and (15) it is reaction (14) that has smallest error and dominates the calculation. Non-ideality in olivine is taken directly from Gudmundsson & Wood (1995), who used a slightly smaller value of $W_{fo,fa}$ than Bryndzia & Wood (1990). Non-ideality in orthopyroxene (see Appendix) makes a small but significant difference to the results, raising calculated log f_{O_2} for reaction (13) by around 0·2 log units. Wood (1990, fig. 2c) showed that an offset of 0·2 log units would produce an almost perfect fit of the barometer equation (13) with his experiments. Thus the new calibration here is in excellent agreement with the 1 bar oxygen sensor measurements. The equations for free energies of reactions (13), (14) and (15) are presented in the Appendix, and computer programs will be made available (from links at http://www.esc.cam.ac.uk/directory/tim-holland) to perform the error propagation of the uncertainties in chemical analyses, the thermodynamic data and the mixing properties of the phases in a least squares optimization of log f_{O_2}.

An important finding of our new calibrations is that, in comparison with earlier parameterizations, the multi-reaction spinel barometry yields log f_{O_2} values that are more reducing by around 0·5 log units. This results from the dominance of the new barometer reaction (14) with its smaller uncertainty and the addition of non-ideal mixing in orthopyroxene. The implications of this and application of both garnet and spinel barometry to mantle peridotites will be explored in the next section.

CAUSES OF DIFFERENCES IN OXYBAROMETERS

There may be several factors that cause differences between the new calibrations of garnet oxybarometers and earlier work. One is the error in the earlier calculation of skiagite free energy as discussed above. Although it is possible that the new skiagite free energy may be uncertain, the high level of agreement between calculations on all three reactions (3), (5) and (6) with the phase equilibrium experiments of Woodland & O'Neill (1993) at all pressures from 27 to 90 kbar at 1100°C suggests that the new data are reliable. The fact that the combined results of four independent reactions, via least squares, yield consistent results within error for well-equilibrated natural samples and most of the experimental samples of Stagno *et al.* (2013) also suggests that the thermodynamic data and phase equilibrium studies on the end-members used are in good agreement. In this context an error of 12 kJ on skiagite free energy, as noted above, would correspond to an error of 23 kbar on the breakdown pressure of skiagite at 1100°C as measured experimentally by Woodland & O'Neill (1993). Their experiments are most unlikely to be in error by that amount.

One possible explanation for the discrepancy may be in the use of oxygen sensor techniques at elevated

pressures. The spinel barometer reaction (13) is in excellent agreement with the 1 atm oxygen sensor measurements of Wood (1990), as shown above, but the garnet equilibria are in less good agreement with the higher pressure oxygen sensor measurements of Gudmundsson & Wood (1995) and Stagno *et al.* (2013). It would appear also that the new calibrations are in much better agreement with the measurements at higher than lower oxygen fugacity, and this might reflect the difficulty of measuring accurately the ferric iron content in garnets at very low concentrations.

APPLICATIONS

A reliable method of calculating f_{O_2} values for mantle peridotites is important for assessing melting, metasomatism and fluid speciation. The use of the oxybarometers presented here requires the measurement of major element oxides for olivine, orthopyroxene, garnet and/or spinel, as well as a *PT* estimate for each xenolith. Because some literature data provide only the Mg-number for olivine and orthopyroxene, the application programs developed here allow for these to be entered in place of a full analysis, and approximate fo, fa, en and fs activities are assigned. It is very important to have an accurate Fe_2O_3 analysis for garnet as this greatly affects the activity of skiagite, and is the last remaining hurdle in accurately calculating f_{O_2} for garnet peridotites.

Variability in the oxidation state of the lithospheric mantle

We have applied the new garnet and spinel oxybarometer calibrations presented above to published data from four mantle xenolith suites. The samples come from a range of tectonic settings—the Baikal Rift (Vitim Volcanic Field; Goncharov & Ionov, 2012) and three major global cratons: Siberian (Udachnaya; Goncharov *et al.*, 2012; Yaxley *et al.*, 2012), Kaapvaal (Woodland & Koch, 2003; Lazarov *et al.*, 2009; Hanger *et al.*, 2015) and Slave (Diavik; McCammon & Kopylova, 2004; Creighton *et al.*, 2009). All these samples have Fe^{3+}/Fe_{total} ratios for pyrope garnets that were measured by Mössbauer spectroscopy, Fe K-edge XANES or the flank method, which currently provide the most accurate values. For internal consistency, we have taken the published analyses of mineral chemistry and recalculated pressures and temperatures using the PTmantle program (Nimis & Grütter, 2010). The following combinations of thermobarometers (with associated errors) were used for the xenolith suites: for garnet lherzolites we used the opx–gt barometer of Nickel & Green (1985; P_{NG85}; ±3 kbar) and the cpx–opx solvus thermometer of Taylor (1998; T_{Ta98}; ±31°C); for garnet harzburgites P_{NG85} was used with the opx–gt thermometer of Nimis & Grütter (2010; T_{NG10}; ±50°C); for spinel lherzolites we have followed Goncharov *et al.* (2012) and extrapolated temperatures, calculated using T_{Ta98}, to the conductive geotherm that was estimated from garnet-bearing samples. We have used our new oxybarometer programs to give revised values of log f_{O_2} relative to the fayalite–magnetite–quartz (FMQ) buffer. For the FMQ buffer we use the expression of O'Neill (1987) with a volume correction from Holland & Powell (2011), as given in the Appendix. Carbon phase stability has then been assessed using log f_{O_2} buffers, calculated using an updated version of the Holland & Powell (2011) dataset, and the relevant conductive geotherms for the various tectonic settings calculated using the GeoTherm program (Mather *et al.*, 2011) for each xenolith suite. A summary of the results is given in Table 3.

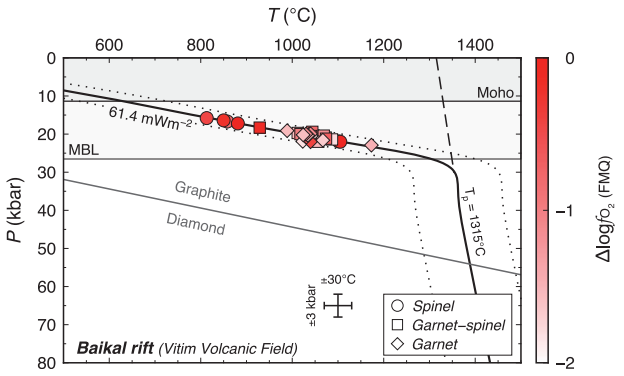

Fig. 4. Plot of pressure vs temperature estimates for off-craton Vitim peridotites from the Baikal Rift zone, using mineral chemistry from Ionov & Wood (1992) and Goncharov & Ionov (2012), together with the thermobarometers of Nickel & Green (1985), Taylor (1998) and Nimis & Taylor (2000). A model conductive geotherm of 61·4 mW m^{-2} has been calculated to best fit the *PT* estimates for garnet-bearing samples in the xenolith suite, using the depth to the Moho of Suvorov *et al.* (2002) and the program described by Mather *et al.* (2011). The diamond–graphite transition (Kennedy & Kennedy, 1976) is indicated, along with a greyscale indication of the Δlog f_{O_2} (FMQ) value for each xenolith. The data indicate that the base of the mechanical boundary layer (MBL) under the Vitim Volcanic Field is relatively shallow at 82 km (26·5 kbar), which is consistent with a previous estimate based on the composition of the host lavas (85 km; Johnson *et al.* 2005).

Baikal Rift (Vitim Volcanic Field)

Spinel- and garnet-bearing mantle peridotites occur in the Vitim Volcanic Field, which is situated to the SE of the Siberian Craton. Our recalculated *PT* estimates for 36 xenoliths analysed by Goncharov & Ionov (2012) show that spinel-only-bearing samples occupy almost the whole depth range (45–65 km) sampled by Vitim magmas (Table 3 and Fig. 4). Because Vitim peridotites contain both garnet and spinel they offer a rare insight into the accuracy of f_{O_2} estimates provided by our new independent oxybarometers. For these samples, our spinel oxybarometer gives Δlog f_{O_2} (FMQ) from –0·43 to +0·20 (av. –0·17), whereas our garnet oxybarometer gives Δlog f_{O_2} (FMQ) in the range –1·79 to –0·14 (av. –1·22). For spinel-only-bearing Vitim peridotites Δlog f_{O_2} (FMQ) estimates range from –1·29 to +0·52 (av. –0·42) and in the spinel-absent garnet-bearing peridotites Δlog f_{O_2} (FMQ) ranges from –1·82 to –0·41 (av. –1·22). A

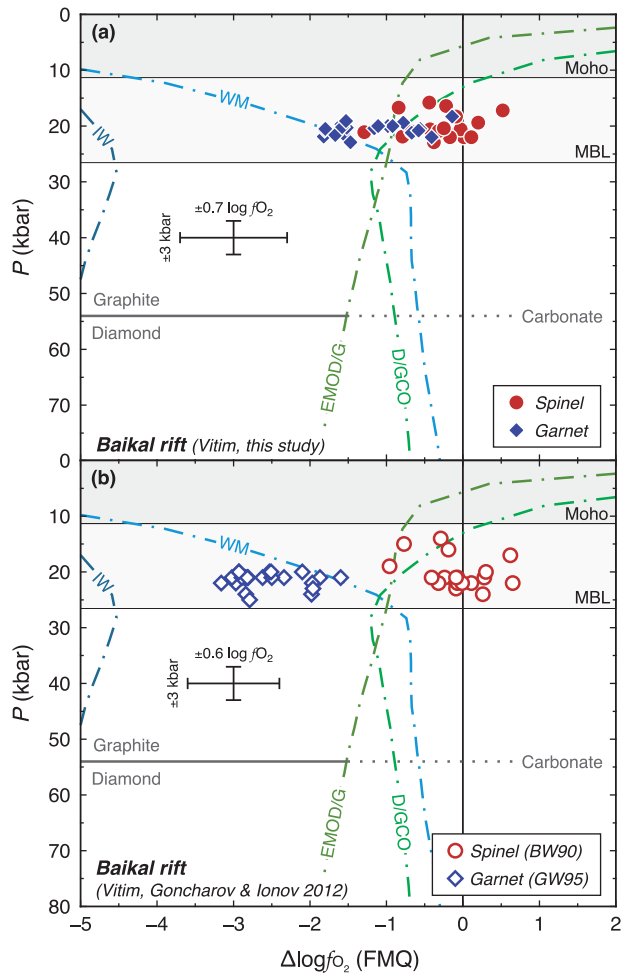

Fig. 5. Plots of Δlog f_{O_2} (FMQ) vs pressure for Vitim peridotites from the Baikal Rift zone: (a) using the oxybarometer calibration from this study; (b) published *P* and f_{O_2} values from Goncharov & Ionov (2012), based on the oxybarometer of Gudmundsson & Wood (1995) (GW95) and the oxybarometer of Bryndzia & Wood (1990) (BW90). Buffer reactions relative to FMQ (fayalite–magnetite–quartz) were calculated from the Holland & Powell (2011) dataset and are as follows: WM, wüstite–magnetite; IW, iron–wüstite; D/GCO, diamond/graphite–CO; EMOD/G, enstatite–magnesite–olivine–diamond/graphite. MBL as in Fig. 4.

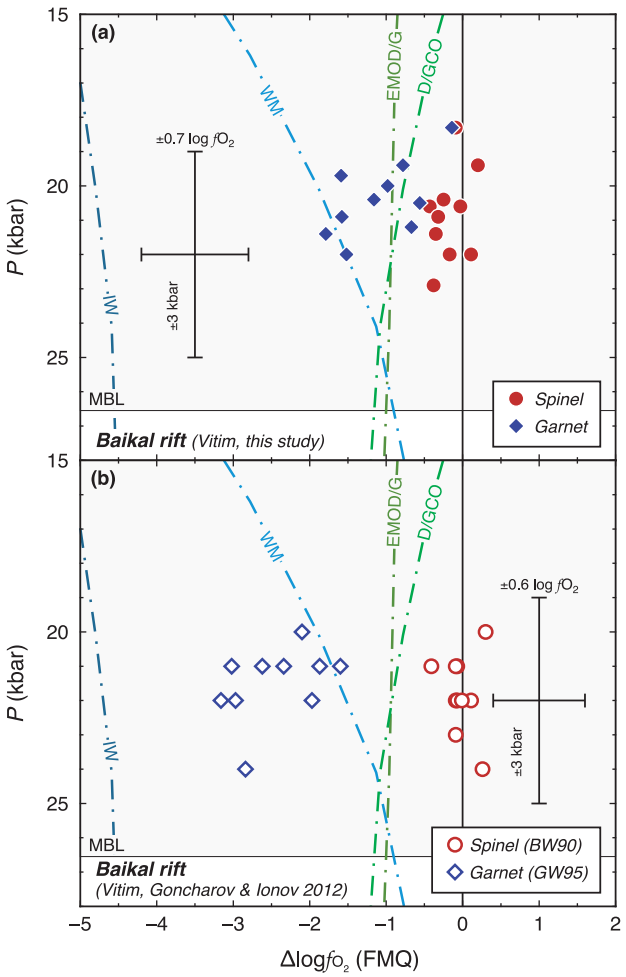

Fig. 6. Plots of Δlog f_{O_2} (FMQ) vs pressure for Vitim spinel–garnet peridotites: (a) using the oxybarometer calibration from this study; (b) published *P* and f_{O_2} values from Goncharov & Ionov (2012), based on the oxybarometer of Gudmundsson & Wood (1995) (GW95) and the oxybarometer of Bryndzia & Wood (1990) (BW90). Buffer reactions are relative to FMQ as in Fig. 5. MBL as in Fig. 4.

comparison of these new values with the published estimates of Goncharov & Ionov (2012) shows that there is a change in spinel-based estimates by –0·2 Δlog f_{O_2} (FMQ) units to more reducing conditions, whereas the garnet-based oxybarometry has increased f_{O_2} estimates by +1·3 Δlog f_{O_2} units. As a consequence the Δlog f_{O_2} (FMQ) values calculated using our new oxybarometers for all samples are in remarkable agreement (Figs 5 and 6), which contrasts with the distinct oxidation states for different assemblages proposed by Goncharov & Ionov (2012). Furthermore, there is no clear variation in Δlog f_{O_2} with depth for the Vitim garnet and spinel peridotites. The wide range in Δlog f_{O_2} (FMQ) (–1·82 to 0·52) over a small pressure range (20–25 kbar) may relate to variable extents of metasomatism by ascending carbonatitic melts at the carbonated peridotite solidus 'ledge' (e.g. Eggler, 1974; Wyllie & Huang, 1976).

Siberian Craton (Udachnaya)

We have used the published data of Yaxley *et al.* (2012) for 18 samples of garnet peridotite and those of Goncharov *et al.* (2012) for 37 samples of spinel- and garnet-bearing peridotites entrained by the Udachnaya kimberlite from the Siberian Craton with our new oxybarometer calibrations. These xenoliths were entrained from a large depth interval (40–210 km; Table 3 and Fig. 7). Spinel- and garnet-bearing samples last equilibrated at depths of 40–100 km and 90–210 km, respectively. Only a few samples (Table 3) contain both aluminous phases. For the Udachnaya spinel peridotites estimates of Δlog f_{O_2} (FMQ) range from –1·71 to –0·09 (av. –0·70). For the deeper garnet peridotites Δlog f_{O_2} (FMQ) ranges from –4·93 to –1·02 (av. –2·01). A comparison of our new values with the published estimates of Goncharov

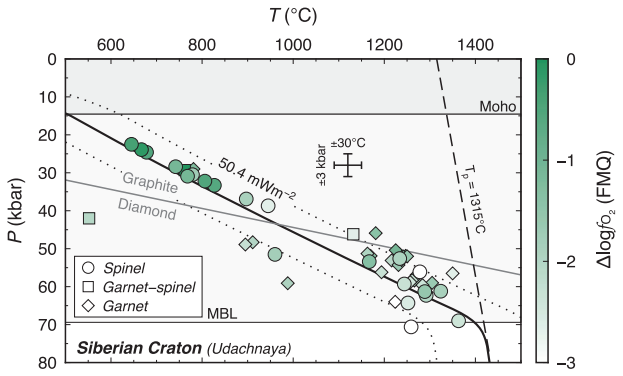

Fig. 7. Pressure vs temperature estimates for Udachnaya peridotites (Siberian Craton). Mineral analyses used for *PT* estimation are from Goncharov *et al.* (2012) using the thermobarometers of Nickel & Green (1985), Taylor (1998), Nimis & Taylor (2000) and Nimis & Grütter (2010). A model conductive geotherm of 50·4 mW m^{-2}was calculated to best fit the *PT* estimates from the xenolith suite, along with the depth to the Moho (Suvorov *et al.*, 2006) using the program described by Mather *et al.* (2011). The estimated mechanical boundary layer (MBL) thickness is 202 km. The diamond–graphite transition pressure (Kennedy & Kennedy, 1976) is indicated, along with a greyscale indication of the Δlog f_{O_2} (FMQ) value for each xenolith.

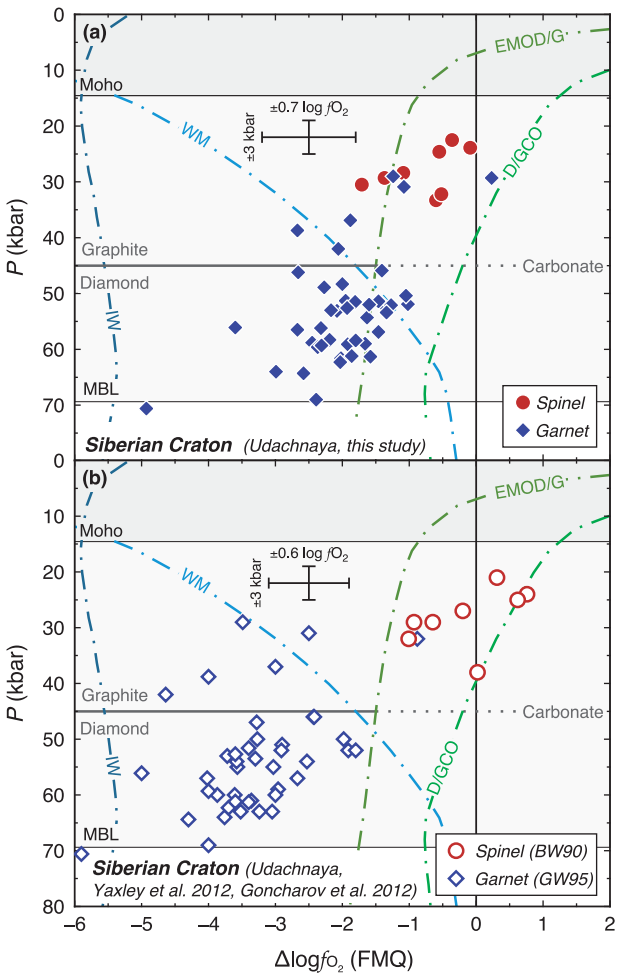

Fig. 8. Plots of Δlog f_{O_2} (FMQ) vs pressure for Udachnaya peridotites (Siberian Craton): (a) using the mineral analyses of Goncharov *et al.* (2012) and Yaxley *et al.* (2012) with the oxybarometer calibration from this study; (b) published *P* and f_{O_2} values from Goncharov *et al.* (2012) and Yaxley *et al.* (2012), based on the oxybarometer of Gudmundsson & Wood (1995) (GW95) and the oxybarometer of Bryndzia & Wood (1990) (BW90). Buffer reactions are relative to FMQ as in Fig. 5. MBL as in Fig. 7.

et al. (2012) and Yaxley *et al.* (2012) shows a change in Δlog f_{O_2} of –0·7 units for spinel-based oxybarometry and +1·3 Δlog f_{O_2} for the garnet-based oxybarometry. The published Δlog f_{O_2} (FMQ) values, together with our recalculated values (Fig. 8), indicate that a number of xenoliths that previously plotted in the diamond stability field now plot at more oxidized conditions on the carbonate stability side of the enstatite–magnesite–olivine–diamond/graphite (EMOD/G) buffer. These more oxidized values agree with the findings of experimental work by Stagno *et al.* (2013), which also suggest that the Gudmundsson & Wood (1995) oxybarometer provides f_{O_2} estimates that are too low. The Udachnaya mantle xenoliths show a clear Δlog f_{O_2} (FMQ) versus depth relationship (Fig. 8). Over a depth range of 165 km, the Δlog f_{O_2} (FMQ) values change from 0·0 at the top of the lithospheric mantle to –3·0 near the base. This gives a lithospheric mantle Δlog f_{O_2} (FMQ) gradient of *c.* 0·18 log units per 10 km, which is lower by 0·07 log units per 10 km than the gradient estimated by Goncharov *et al.* (2012).

Kaapvaal Craton

We have used published analyses of mineral phases present in 16 peridotites from the Finsch mine, South Africa (Lazarov *et al.*, 2009) and 53 peridotite xenoliths from the wider Kaapvaal Craton (Woodland & Koch, 2003; Hanger *et al.*, 2015) to estimate equilibration pressures and temperatures together with f_{O_2}. All samples are garnet bearing and cover a large depth range (75–190 km; Table 3 and Fig. 9). All of the Finsch garnet-bearing peridotites have f_{O_2} estimates that range from –3·78 to –1·87 Δlog f_{O_2} (FMQ) (av. –2·61). The other Kaapvaal xenoliths have f_{O_2} estimates that range from –2·94 to –0·67 Δlog f_{O_2} (FMQ) (av. –2·09).

A comparison (Fig. 10) of the f_{O_2} values calculated by Lazarov *et al.* (2009), who used the calibration of Gudmundsson & Wood (1995) as corrected by Woodland & Peltonen (1999), with recalculated values for the same xenoliths using our new oxybarometers indicates a shift in f_{O_2} estimates of +1·0 Δlog f_{O_2} (FMQ) units. The same shift in f_{O_2} estimates is also seen for the other Kaapvaal xenoliths. Moreover, garnet lherzolites from across the entire craton give a lithospheric mantle gradient of 0·24 Δlog f_{O_2} (FMQ) per 10 km, whereas garnet harzburgites indicate a lithospheric gradient of 0·29 Δlog f_{O_2} (FMQ) per 10 km, which is similar to the estimate of Lazarov *et al.* (2009). Reassuringly, both diamond-bearing samples plot in the diamond stability field. The relatively large spread of f_{O_2} that is observed at depth in the Kaapvaal

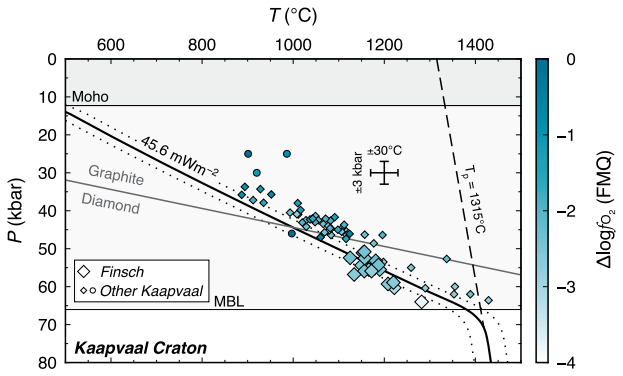

Fig. 9. Pressure vs temperature estimates for peridotites from the Kaapvaal Craton. Circles, spinel-bearing samples; diamonds, garnet-bearing samples. Mineral analyses are from Woodland & Koch (2003) and Lazarov *et al.* (2009). Pressures and temperatures were estimated using the thermobarometers of Nickel & Green (1985), Taylor (1998) and Nimis & Grütter (2010). A model conductive geotherm of 45·6 mW m^{-2} has been calculated to best fit the *PT* estimates from the Finsch xenolith suite, along with the depth to the Moho (Nair *et al.*, 2006) using the program described by Mather *et al.* (2011). The estimated thickness of the mechanical boundary layer (MBL) is 204 km. This is in reasonable agreement with published findings for Finsch (Gibson *et al.*, 2008; Lazarov *et al.*, 2009). The diamond–graphite transition (Kennedy & Kennedy, 1976) is shown, along with a greyscale indication of the Δlog f_{O_2} (FMQ) value for each xenolith.

lithosphere may reflect variable metasomatic enrichment over short length scales.

Slave Craton (Diavik Mine)

Analyses of mineral phases present in 69 garnet-bearing mantle peridotites from Diavik Mine, central Slave Craton have been used to calculate final equilibration pressures and temperatures with the P_{NG85} barometer and the T_{Ta98} thermometer (Table 3 and Fig. 11). Creighton *et al.* (2009) presented two sets of *PT* estimates for these same xenoliths: one using the Brey & Köhler (1990) barometer (P_{BKN}) and thermometer (T_{BKN}); the other using the thermometer of O'Neill & Wood (1979; T_{OW}) in combination with P_{BKN}. The *PT* estimates using the P_{BKN} and T_{OW} combination were lower than the P_{BKN} and T_{BKN} combination. Our recalculations agree more closely with the P_{BKN} and T_{BKN} combination. Based on these calculations, most of the xenoliths were entrained from 150 to 190 km with a few additional samples from 125 to 135 km.

Using our new oxybarometers, estimates of Δlog f_{O_2} (FMQ) for Diavik garnet peridotites range from –3·73 to +0·03 (av. –1·68), which is an increase of +1·4 Δlog f_{O_2} (FMQ) units compared with the previous Gudmundsson & Wood (1995) calibration. This range in f_{O_2} occurs in the lower half of the cratonic lithosphere, and has had the effect of moving half of the xenolith samples out of the diamond stability field, crossing the wüstite–magnetite (WM) and EMOD/G buffers to more oxidizing conditions (Fig. 12). The large range in f_{O_2} for the lithospheric mantle beneath the central Slave Craton is similar to that for the Siberian Craton (Udachnaya; Fig. 8).

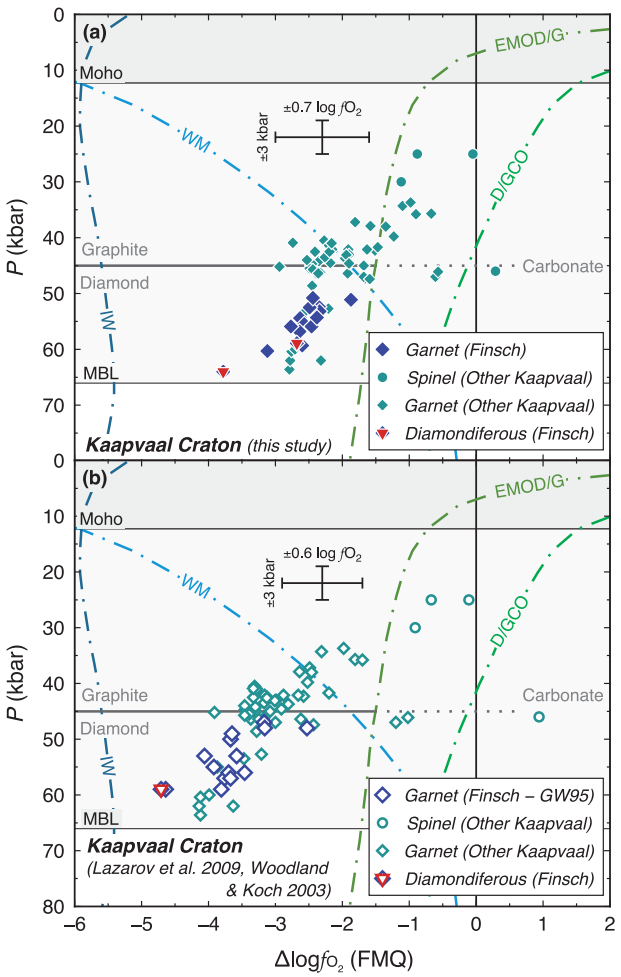

Fig. 10. Variation of Δlog f_{O_2} (FMQ) vs pressure for Finsch and other Kaapvaal garnet-peridotites: (a) using the mineral analyses of Woodland & Koch (2003) and Lazarov *et al.* (2009), and the oxybarometer calibration from this study; (b) published *P* and f_{O_2} values from Woodland & Koch (2003) and Lazarov *et al.* (2009). Buffer reactions are relative to FMQ as in Fig. 5. It should be noted that Lazarov *et al.* (2009) did not publish f_{O_2} values for all 28 xenoliths. MBL as in Fig. 9.

Small-scale variability of f_{O_2}: an example from the Kaapvaal Craton

The variations in f_{O_2} that we have described above represent changes in oxidation state of the lithospheric mantle over large depth intervals. Localized interactions between percolating metasomatizing melts and existing mineral phases, immediately prior to or during entrainment, may also cause micro-scale changes in f_{O_2}. Although high-quality garnet Fe_2O_3 data are limited for such samples, Berry *et al.* (2013) made observations and calculations on a single zoned garnet from a Kaapvaal mantle peridotite, using the compositions of the core and the rim to deduce their separate *PT* and f_{O_2} conditions. They assumed that the core of the garnet was in equilibrium with the surrounding orthopyroxene, and calculated a pressure of 47 kbar (P_{NG85}) and temperature of 1060°C with the Canil (1994) thermometer. Our *PT* recalculation using P_{NG85} and T_{Ta98} for both

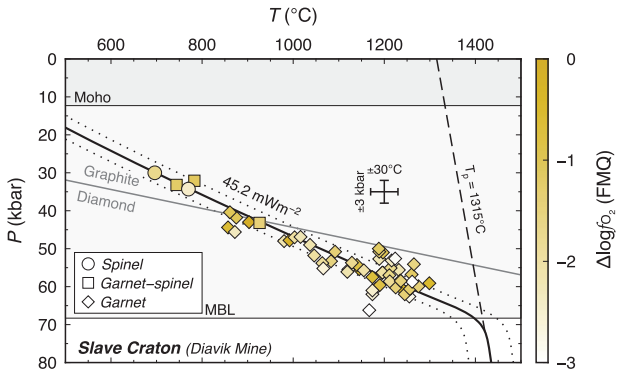

Fig. 11. Pressure vs temperature estimates for Diavik peridotites (Slave Craton). Mineral analyses from McCammon & Kopylova (2004) and Creighton *et al.* (2009) were used with the thermobarometers of Nickel & Green (1985), Taylor (1998) and Nimis & Grütter (2010). A model conductive geotherm of 45·2 mW m^{-2} has been calculated to best fit the *PT* estimates from the xenolith suite, along with the depth to the Moho (Bank *et al.*, 2000) using the program described by Mather *et al.* (2011). The estimated thickness of the mechanical boundary layer (MBL) beneath the central Slave Craton is 211 km. The diamond–graphite transition pressure (Kennedy & Kennedy, 1976) is indicated, along with a greyscale indication of the Δlog f_{O_2} (FMQ) value for each xenolith. It should be noted that McCammon & Kopylova (2004) assumed a pressure of 30 kbar for the spinel-only peridotites.

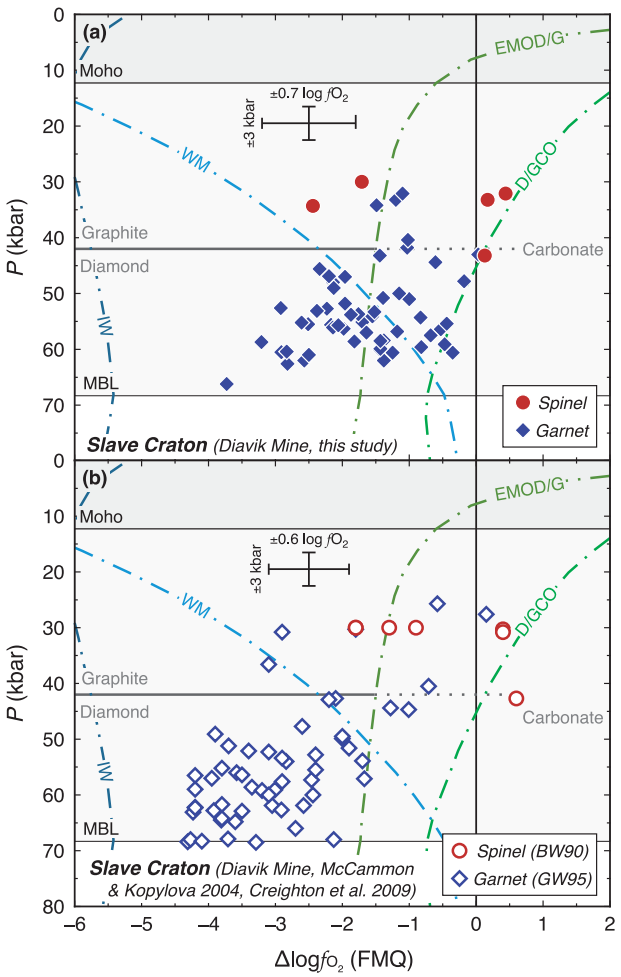

Fig. 12. Variation of Δlog f_{O_2} (FMQ) vs pressure for Diavik peridotites (Slave Craton): (a) using the mineral analyses of Creighton *et al.* (2009) and the oxybarometer calibration from this study; (b) published *P* and f_{O_2} values from McCammon & Kopylova (2004) and Creighton *et al.* (2009), based on the oxybarometers of Bryndzia & Wood (1990) (BW90) and Gudmundsson & Wood (1995) (GW95). Buffer reactions as in Fig. 5.

garnet core and rim oxide data from Berry *et al.* (2013) gave revised estimates of 50·6 kbar and 1061°C for the core, and 50·0 kbar and 1059°C for the rim. Although identical to the results of Berry *et al.* (2013), it should be noted that the PTmantle program (Nimis & Grütter, 2010) suggests orthopyroxene–clinopyroxene disequilibrium errors for both estimates, and a garnet–pyroxene disequilibrium error for the core calculation.

Our new oxybarometer calibration gives estimates of Δlog f_{O_2} (FMQ) = –1·59 for the garnet core and –0·57 for the rim compositions. This increase in Δlog f_{O_2} (FMQ) of +0·8 for the core and +0·5 for the rim places the rim firmly in the carbonate stability field whereas the core moves to the EMOD/G buffer, making diamond stability questionable. Nevertheless, the oxybarometer presented here, and in earlier versions (Gudmundsson & Wood, 1995; Woodland & Peltonen, 1999), relies on the assumption that the phases used in the calculation were in equilibrium. It seems likely that either the core or the rim of the garnet, being compositionally different, was not in equilibrium with the xenolith assemblage. This is most probably due to cryptic metasomatism of the garnet rim, either immediately prior to or during entrainment.

Relative effects of *P* and ferric ratio of garnet on calculated log f_{O_2}

The relative effects of pressure and ferric ratio ($f = Fe^{3+}/\sum Fe$) of garnet on log f_{O_2} are investigated for a particular peridotite sample, along an imposed mantle geotherm. For this example, sample Y17 from Udachnaya (Siberian Craton, Table 3) was selected. The lithospheric geotherm of 50·4 mW m^{-2} from Fig. 7 was used and these conditions are represented as *T* (°C) = 252 + 17·39*P* (kbar). Total Fe in sample Y17 garnet was maintained, but the ferric ratio *f* was varied from 0·03 to 0·12, a range typical of mantle xenolith samples (e.g. Woodland & Koch, 2003, fig. 3). Compositions of olivine and orthopyroxene were kept constant, a procedure that leads to imperceptible error. Because Fe and Mg in garnet depend on the garnet–olivine exchange equilibrium, the Fe/Mg ratio was adjusted at each temperature and pressure along the geotherm using the values of K_d from O'Neill & Wood (1979). Concentrations of other elements in garnet were held constant. Figure 13 shows the results of applying the multi-reaction oxybarometry to Y17 in the range 30–60 kbar along the geotherm, for four chosen values of *f*. As expected, calculated values of log f_{O_2} decrease with increasing pressure, with the smallest *f* yielding the most reduced

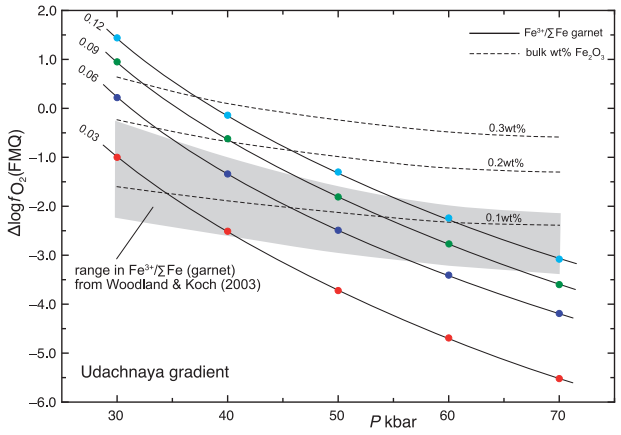

Fig. 13. Variation of $\Delta\log f_{O_2}$ (FMQ) vs pressure along the mantle geotherm from Fig. 7 for peridotite sample Y17 from Udachnaya (Siberian Craton, Table 3) using four values of $Fe^{3+}/\sum Fe$ in garnet. Details are discussed in the text. The shaded field corresponds to the range in measured mantle $Fe^{3+}/\sum Fe$ in garnet from Woodland & Koch (2003) and the dashed lines are calculated for the Y17 bulk composition, with three Fe_2O_3 contents using the thermodynamic model from Jennings & Holland (2015).

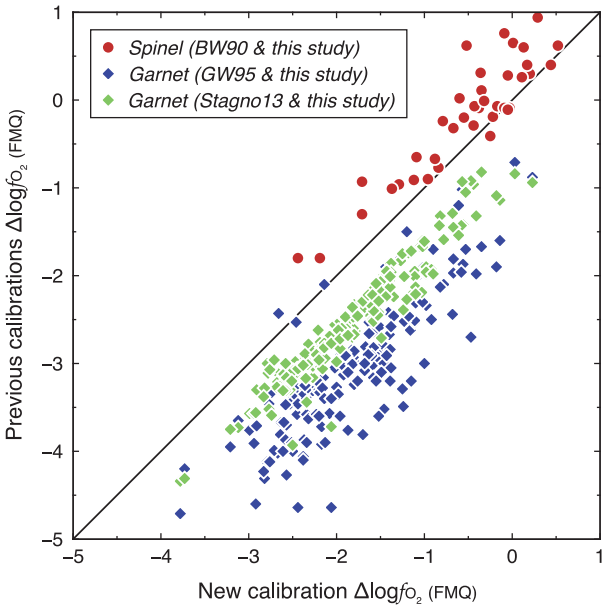

Fig. 14. A summary plot comparing recalibrated oxygen fugacities with earlier studies for all peridotites in this study. For spinel-bearing peridotites (circles) the oxygen fugacities are 0–1 log units more reduced than those estimated by the Bryndzia & Wood (1990, BW90) barometer; for garnet-bearing peridotites the largest change is relative to the Gudmundsson & Wood (1995, GW95) barometer (black diamonds), which shows more reduced oxygen fugacities by 0–2·5 log units, whereas the barometer of Stagno *et al.* (2013, Stagno13) lies closer to the present results (grey diamonds) but is displaced to more reducing conditions by 0·2–1·5 log units, values that are within the combined uncertainty of measurements and barometers.

values. It is well known (e.g. Woodland & Koch, 2003) that *f* increases with temperature (and hence pressure via the imposed geotherm) such that the deepest samples will be less reduced than shown by extrapolating along lines of constant *f*. The shaded region in Fig. 13 corresponds to the range in *f* from fig. 3 of Woodland & Koch (2003) and has a shallower slope than the constant *f* isopleths. In these calculations the garnet composition was not varied, except for allowing changes to the ferric iron via the parameter *f* and adjustment of Fe/Mg ratios at constant Ca to satisfy garnet–olivine equilibrium. Garnet in sample Y17 contains 4·8 wt % Cr_2O_3, a value slightly smaller than the median of the observed range in this study (maximum around 12 wt % Cr_2O_3). Exchanging Cr_2O_3 for Al_2O_3 in garnet to cover the range 0–12 wt % Cr_2O_3 was found to make less than 0·1 log unit log f_{O_2} difference to the results shown.

Also shown in Fig. 13 are calculated curves for three assigned values of Fe_2O_3 for the Y17 bulk composition, using the thermodynamic model of Jennings & Holland (2015), to indicate the effects of changing the bulk ferric iron content. The constant bulk composition slopes are significantly shallower than the *f* isopleths and flatten off to almost constant log f_{O_2} at high pressures. They also match the slope of the shaded region reasonably well. It is important to keep in mind the very different nature of the information in Fig. 13: the isopleths of *f* are based on oxybarometry on a natural sample, whereas the constant ferric bulk composition curves are predictions from a thermodynamic model using the same sample bulk composition. The measured log f_{O_2} values for Udachnaya, as seen in Fig. 8, suggest a change from –1 to –3 log units over this pressure range, in good agreement with the shaded region in Fig. 13. A comparison with fig. 14 of Jennings & Holland (2015) suggests that a mantle with a composition similar to fertile peridotite KLB-1 (Takahashi, 1986), with around 0·2 wt % Fe_2O_3, can satisfactorily explain the bulk of mantle xenolith data, whereas depleted mantle peridotites may be characterized by slightly lower bulk Fe_2O_3 contents. Values of log f_{O_2} in natural samples appear to be closely controlled by relatively constant composition. The variation in *f* from 0·03 to 0·12 at any pressure along the geotherm in Fig. 13 leads to changes of around 2·5 log f_{O_2} units.

CONCLUSIONS

Assuming that all phases are in equilibrium within a spinel- and garnet-bearing peridotite, it is expected that f_{O_2} estimates from the two independent spinel-based and garnet-based oxybarometers will give the same value. Our revision of the spinel- and garnet-based oxybarometers has changed estimates of f_{O_2} for both oxybarometers. As detailed above, spinel-based estimates are now more reduced, whereas garnet-based estimates are more oxidized, leading to a reduced discrepancy between the two methods by around 2·0 $\Delta\log f_{O_2}$ units. Figures 5, 6 and 8 show the effect that recalibration has had on f_{O_2} estimates in resolving the discrepancy between spinel- and garnet-based oxybarometers. In Fig. 6 all the spinel- and garnet-bearing peridotites now cluster around the wüstite–magnetite (WM) and enstatite–magnesite–olivine–diamond/graphite (EMOD/

G) buffers. Further conclusions from this work are as follows.

1. Recalibration of the Gudmundsson & Wood (1995) skiagite oxygen barometer using (a) the recalculation of skiagite free energy derived from the experimental data of Woodland & O'Neill (1993) and (b) the recalibration of the garnet mixing model has shifted garnet-based oxybarometer f_{O_2} estimates to more oxidized values by *c.* 0·70–1·5 $\Delta\log f_{O_2}$ (FMQ) units (Fig. 14). This shift to more oxidized conditions has moved f_{O_2} estimates away from the iron–wüstite (IW) buffer, and hence away from the highly reducing conditions necessary for metal saturation at the base of the lithosphere.
2. Several xenoliths previously thought to have originated from the diamond stability field may have experienced more oxidizing conditions, placing them above the WM and EMOD/G buffers, where carbonate is the stable carbon phase. Known diamondiferous xenoliths from Finsch Mine remain within the diamond stability field (within error) (Fig. 10).
3. Revision of spinel oxybarometry in combination with our new garnet oxybarometer calibration reduces the difference between spinel- and garnet-based f_{O_2} estimates for mantle peridotites. The revised spinel oxybarometer now gives slightly more reduced f_{O_2} values, by *c.* 0·7 $\Delta\log f_{O_2}$ units (Fig. 14).
4. Peridotites with coexisting spinel and garnet from the Vitim Volcanic Field (Baikal Rift, Russia) now show similar f_{O_2} values for the two independent methods, but whether they should be identical remains questionable.
5. Introduction of multi-reaction oxybarometry for spinel and garnet peridotites increases the robustness of the estimation process and allows assessment of the possible disequilibrium in mantle samples.
6. Accurate and reliable measurement of Fe_2O_3, from $Fe^{3+}/\sum Fe$ ratios, remains the last hurdle in reliable oxygen fugacity calculation, as the amount of Fe_2O_3 greatly affects the activity of skiagite, and hence the f_{O_2} value calculated.

ACKNOWLEDGEMENTS

We are grateful to Eve Rooks for helpful discussions on thermobarometry, and to Paolo Nimis for providing a copy of the *P–T* mantle spreadsheet. This research builds on the findings of work carried out by W.M. for his MSc project at the University of Cambridge. We are grateful to Dan Frost and several anonymous reviewers who contributed significantly to improvement of the paper.

FUNDING

This work was supported by a Natural Environment Research Council studentship [NE/L501578/1] to W. Miller.

REFERENCES

Bank, C. G., Bostock, M. G., Ellis, R. M. & Cassidy, J. F. (2000). A reconnaissance teleseismic study of the upper mantle and transition zone beneath the Archean Slave craton in NW Canada. *Tectonophysics* **319**, 151–166.

Berry, A. G., Yaxley, G. M., Hanger, B. J., Woodland, A. B., de Jonge, M. D., Howard, D. L., Paterson, D. & Kamenetsky, V. S. (2013). Quantitative mapping of the oxidative effects of mantle metasomatism. *Geology* **41**, 683–686.

Brey, G. P. & Köhler, T. (1990). Geothermobarometry in four-phase lherzolites. II. New thermobarometers, and practical assessment of existing thermobarometers. *Journal of Petrology* **31**, 1353–1378.

Bryndzia, L. T. & Wood, B. J. (1990). Oxygen thermobarometry of abyssal spinel peridotites: the redox state and C–O–H volatile composition of the Earth's sub-oceanic upper mantle. *American Journal of Science* **290**, 1093–1116.

Canil, D. (1994). An experimental calibration of the 'Nickel in Garnet' geothermometer with applications. *Contributions to Mineralogy and Petrology* **117**, 410–420.

Canil, D. & O'Neill, H. St. C. (1996). Distribution of ferric iron in some upper-mantle assemblages. *Journal of Petrology* **37**, 609–635.

Creighton, S., Stachel, T., Matveev, S., Höfer, H., McCammon, C. & Luth, R. W. (2009). Oxidation of the Kaapvaal lithospheric mantle driven by metasomatism. *Contributions to Mineralogy and Petrology* **157**, 491–504.

Dachs, E., Geiger, C. A. & Benisek, A. (2012). Almandine: Lattice and non-lattice heat capacity behavior and standard thermodynamic properties. *American Mineralogist* **97**, 1771–1782.

Dasgupta, R. & Hirschmann, M. M. (2010). The deep carbon cycle and melting in Earth's interior. *Earth and Planetary Science Letters* **298**, 1–13.

Davies, P. K. & Navrotsky, A. (1983). Quantitative correlations of deviations from ideality in binary and pseudo-binary solid solutions. *Journal of Solid State Chemistry* **46**, 1–22.

Eggler, D. H. (1974). Effect of CO_2 on the melting of peridotite. *Carnegie Institution of Washington Yearbook* **73**, 215–224.

Foley, S. F. (2010). A reappraisal of redox melting in the Earth's mantle as a function of tectonic setting and time. *Journal of Petrology* **10**, 1–29.

Frost, D. & McCammon, C. (2008). The redox state of Earth's mantle. *Annual Review of Earth and Planetary Sciences* **36**, 389–420.

Ganguly, J., Cheng, W. & Tirone, M. (1996). Thermodynamics of aluminosilicate garnet solid solution, new experimental data, an optimized model, and thermometric applications. *Contributions to Mineralogy and Petrology* **126**, 137–151.

Geiger, C. A., Newton, R. C. & Kleppa, O. J. (1987). Enthalpy of mixing of synthetic almandine–grossular and almandine–pyrope garnets from high-temperature solution calorimetry. *Geochimica et Cosmochimica Acta* **51**, 1755–1763.

Gibson, S. A., Malarkey, J. & Day, J. A. (2008). Melt depletion and enrichment beneath the western Kaapvaal craton: Evidence from Finsch peridotite xenoliths. *Journal of Petrology* **49**, 1817–1852.

Goncharov, A. G. & Ionov, D. A. (2012). Redox state of deep off-craton lithospheric mantle: new data from garnet and spinel peridotites from Vitim, southern Siberia. *Contributions to Mineralogy and Petrology* **164**, 731–745.

Goncharov, A. G., Ionov, D. A., Doucet, L. S. & Pokhilenko, L. N. (2012). Thermal state, oxygen fugacity and C–O–H fluid speciation in cratonic lithospheric mantle: New data on peridotite xenoliths from the Udachnaya kimberlite, Siberia. *Earth and Planetary Science Letters* **357–358**, 99–110.

Green, E. C. R., Holland, T. J. B., Powell, R. & White, R. W. (2012). Garnet and spinel lherzolite assemblages in MgO–

Al_2O_3–SiO_2 and CaO–MgO–Al_2O_3–SiO_2: thermodynamic models and an experimental conflict. *Journal of Metamorphic Geology* **30**, 561–577.

Gudmundsson, G. & Wood, B. J. (1995). Experimental tests of garnet peridotite oxygen barometry. *Contributions to Mineralogy and Petrology* **119**, 56–67.

Hackler, R. T. & Wood, B. J. (1989). Experimental determination of Fe and Mg exchange between garnet and olivine and estimation of Fe–Mg mixing properties in garnet. *American Mineralogist* **74**, 994–999.

Hanger, B. J., Yaxley, G. M., Berry, A. J. & Kamenesky, V. S. (2015). Relationships between oxygen fugacity and metasomatism in the Kaapvaal subcratonic mantle, represented by garnet peridotite xenoliths in the Wesselton kimberlite, South Africa. *Lithos* **212–215**, 443–452.

Harte, B. (2010). Diamond formation in the deep mantle: the record of mineral inclusions and their distribution in relation to mantle dehydration zones. *Mineralogical Magazine* **74**, 189–215.

Harte, B. & Cayser, N. (2007). Decompression and unmixing of crystals included in diamonds from the mantle transition zone. *Physics and Chemistry of Minerals* **34**, 647–656.

Holdaway, M. J. (1972). Thermal stability of Al–Fe epidote as a function of f_{O2} and Fe content. *Contributions to Mineralogy and Petrology* **37**, 307–340.

Holland, T. J. B. & Powell, R. (1990). An enlarged and updated internally consistent thermodynamic dataset with uncertainties and correlations: the system K_2O–Na_2O–CaO–MgO–MnO–FeO–Fe_2O_3–Al_2O_3–TiO_2–SiO_2–C–H_2–O_2. *Journal of Metamorphic Geology* **8**, 89–124.

Holland, T. J. B. & Powell, R. (2011). An improved and extended internally consistent thermodynamic dataset for phases of petrological interest, involving a new equation of state for solids. *Journal of Metamorphic Geology* **29**, 333–383.

Holmes, R. D., O'Neill, H. St. C. & Arculus, R. J. (1986). Standard Gibbs free energy of formation for Cu,O, NiO, CoO, and FeO: High resolution electrochemical measurements using zirconia solid electrolytes from 900–1400 K. *Geochimica et Cosmochimica Acta* **50**, 2439–2452.

Huckenholz, H. G. & Knittel, D. (1975). Uvarovite: Stability of uvarovite–grossularite solid solution at low pressure. *Contributions to Mineralogy and Petrology* **49**, 211–232.

Ionov, D. A. & Wood, B. J. (1992). The oxidation state of subcontinental mantle: oxygen thermobarometry of mantle xenoliths from central Asia. *Contributions to Mineralogy and Petrology* **111**, 179–193.

Ionov, D. A., Ashchepkov, I. & Jagoutz, E. (2005). The provenance of fertile off-craton lithospheric mantle: Sr–Nd isotope and chemical composition of garnet and spinel peridotite xenoliths from Vitim, Siberia. *Chemical Geology* **217**, 41–75.

Ionov, D. A., Doucet, L. S. & Ashchepkov, I. V. (2010). Composition of the lithospheric mantle in the Siberian Craton; new constraints from fresh peridotites in the Udachnaya-East Kimberlite. *Journal of Petrology* **51**, 2177–2210.

Jennings, E. S. & Holland, T. J. B. (2015). A simple thermodynamic model for melting of peridotite in the system NCFMASOCr. *Journal of Petrology* **56**, 869–892.

Johnson, J., Gibson, S. A., Thompson, R. N. & Nowell, G. M. (2005). Volcanism in the Vitim Field, Siberia: geochemical evidence for a mantle plume beneath the Baikal Rift Zone. *Journal of Petrology* **46**, 1309–1344.

Kennedy, C. S. & Kennedy, G. C. (1976). The equilibrium boundary between graphite and diamond. *Journal of Geophysical Research* **81**, 2467–2470.

Klemme, S., van Miltenburg, J. C., Javorsky, P. & Wastin, F. (2005). Thermodynamic properties of uvarovite garnet ($Ca_3Cr_2Si_3O_{12}$). *American Mineralogist* **90**, 663–666.

Kopylova, M. G. & Caro, G. (2004). Mantle xenoliths from the south-eastern Slave craton: Evidence from chemical zonation in a thick, cold lithosphere. *Journal of Petrology* **45**, 1045–1067.

Kopylova, M. G., Russell, J. K. & Cookenboo, H. (1999). Petrology of peridotite and pyroxenite xenoliths from the Jericho kimberlite: implications for the thermal state of the mantle beneath the Slave craton, northern Canada. *Journal of Petrology* **40**, 79–104.

Koziol, A. M. (1990). Activity–composition relationships of binary Ca–Fe and Ca–Mn garnets determined by reversed, displaced equilibrium experiments. *American Mineralogist* **75**, 319–327.

Koziol, A. M. & Bohlen, S. R. (1992). Solution properties of almandine–pyrope garnet as determined by phase equilibrium experiments. *American Mineralogist* **77**, 765–773.

Lazarov, M., Woodland, A. B. & Brey, G. P. (2009). Thermal state and redox conditions of the Kaapvaal mantle: a study of xenoliths from the Finsch mine, South Africa. *Lithos* **112**, 913–923.

Leger, J. M., Redon, A. M. & Chateau, C. (1990). Compressions of synthetic pyrope, spessartine and uvarovite garnets up to 25 GPa. *Physics and Chemistry of Minerals* **17**, 161–167.

Luth, R. W., Virgo, D., Boyd, F. R. & Wood, B. J. (1990). Ferric iron in mantle-derived garnets. Implications for thermobarometry and for the oxidation state of the mantle. *Contributions to Mineralogy and Petrology* **104**, 56–72.

Mather, K. A., Pearson, D. G., McKenzie, D. P., Kjarsgaard, B. A. & Priestly, K. (2011). Constraints on the depth and thermal history of cratonic lithosphere from peridotite xenoliths, xenocrysts and seismology. *Lithos* **125**, 729–742.

Mattioli, G. S. & Bishop, F. C. (1984). Experimental determination of the chromium–aluminum mixing parameter in garnet. *Geochimica et Cosmochimica Acta* **48**, 1367–1371.

McCammon, C. & Kopylova, M. G. (2004). A redox profile of the Slave mantle and oxygen fugacity control in the cratonic mantle. *Contributions to Mineralogy and Petrology* **148**, 55–68.

Nair, S. K., Gao, S. S., Liu, K. H. & Silver, P. G. (2006). Southern African crustal evolution and composition: Constraints from receiver function studies. *Journal of Geophysical Research: Solid Earth* **111**, B02304.

Navrotsky, A. (1986). Cation distribution energetics and heats of mixing in $MgFe_2O_4$–$MgAl_2O_4$, $ZnFe_2O_4$–$ZnAl_2O_4$, and $NiAl_2O_4$–$ZnAl_2O_4$ spinels, study by high temperature calorimetry. *American Mineralogist* **71**, 1160–1169.

Newton, R. C., Charlu, T. V. & Kleppa, O. J. (1977). Thermochemistry of high-pressure garnets and clinopyroxenes in the system CaO–MgO–Al_2O_3–SiO_2. *Geochimica et Cosmochimica Acta* **41**, 369–377.

Nickel, K. G. & Green, D. H. (1985). Empirical geothermobarometry for garnet peridotites and implications for the nature of the lithosphere, kimberlites and diamonds. *Earth and Planetary Science Letters* **73**, 158–170.

Nimis, P. & Gruütter, H. (2010). Internally consistent geothermometers for garnet peridotites and pyroxenites. *Contributions to Mineralogy and Petrology* **159**, 411–427.

Nimis, P. & Taylor, W. R. (2000). Single-clinopyroxene thermobarometry for garnet peridotites. Part I. Calibration and testing of a Cr-in-Cpx barometer and an enstatite-in-Cpx thermometer. *Contributions to Mineralogy and Petrology* **139**, 541–554.

O'Neill, H. St. C. (1987). Quartz–fayalite–iron and quartz–fayalite–magnetite equilibria and the free energy of formation of fayalite (Fe_2SiO_4) and magnetite (Fe_3O_4). *American Mineralogist* **72**, 67–75.

O'Neill, H. St. C. & Navrostky, A. (1983). Simple spinels: crystallographic parameters, cation radii, lattice energies, and cation distributions. *American Mineralogist* **68**, 181–194.

O'Neill, H. St. C. & Wood, B. J. (1979). An experimental study of Fe–Mg-partitioning between garnet and olivine and its calibration as a geothermometer. *Contributions to Mineralogy and Petrology* **70**, 59–70.

Ottonello, G., Bokreta, M. & Sciuto, P. F. (1996). Parameterization of energy and interactions in garnets: End-member properties. *American Mineralogist* **81**, 429–447.

Petric, A., Jacob, K. T. & Alcock, C. B. (1981). Thermodynamic properties of Fe_3O_4–$FeAl_2O_4$ spinel solid solutions. *Journal of the American Ceramic Society* **64**, 632–639.

Powell, R. & Holland, T. J. B. (1988). An internally consistent thermodynamic dataset with uncertainties and correlations: 3. Application methods, worked examples and a computer program. *Journal of Metamorphic Geology* **6**, 173–204.

Powell, R. & Holland, T.J. B. (1993). On the formulation of simple mixing models for complex phases. *American Mineralogist* **78**, 1174–1180.

Powell, R. & Holland, T. J. B. (1994). Optimal geothermometry and geobarometry. *American Mineralogist* **79**, 120–133.

Powell, R. & Holland, T. J. B. (1999). Relating formulations of the thermodynamics of mineral solid solutions; activity modeling of pyroxenes, amphiboles, and micas. *American Mineralogist* **84**, 1–14.

Pownceby, M. I., Wall, V. J. & O'Neill, H. St. C. (1987). Fe–Mn partitioning between garnet and ilmenite: experimental calibration and applications. *Contributions to Mineralogy and Petrology* **97**, 116–126.

Robie, R. A. & Hemingway, B. S. (1995). *Thermodynamic properties of minerals and related substances at 298·15 K and 1 bar (105 Pascals) pressure and at higher temperatures. US Geological Survey Bulletin* **2131**, 461 pp.

Stagno, V., Ojwang, D. O., McCammon, C. A. & Frost, D. J. (2013). The oxidation state of the mantle and the extraction of carbon from Earth's interior. *Nature* **493**, 84–89.

Suvorov, V. D., Mishenkina, Z. M., Petrick, G. V., Sheludko, I. F., Seleznev, V. S. & Solovyov, V. M. (2002). Structure of the Baikal rift zone and adjacent areas from deep seismic sounding data. *Tectonophysics* **351**, 61–74.

Suvorov, V. D., Melnik, E. A., Thybo, H., Perchuc, E. & Parasotka, B. S. (2006). Seismic velocity model of the crust and uppermost mantle around the Mirnyi kimberlite field in Siberia. *Tectonophysics* **420**, 49–73.

Takahashi, E. (1986). Melting of a dry peridotite KLB-1 up to 14 GPa: implications on the origin of peridotitic upper mantle. *Journal of Geophysical Research* **91**, 9367–9382.

Taylor, W. R. (1998). An experimental test of some geothermometer and geobarometer formulations for upper mantle peridotites with application to the thermobarometry of fertile lherzolite and garnet websterite. *Neues Jahrbuch für Mineralogie, Abhandlungen* **172**, 381–408.

Turnock, A. C. & Eugster, H. P. (1962). Fe–Al oxides: phase relationships below 1000°C. *Journal of Petrology* **3**, 533–565.

Wijbrans, C. J., Niehaus, O., Rohrbach, A., Pöttgen, R. & Klemme, S. (2014). Thermodynamic and magnetic properties of knorringite garnet ($Mg_3Cr_2Si_3O_{12}$) based on low-temperature calorimetry and magnetic susceptibility measurements. *Physics and Chemistry of Minerals* **41**, 341–346.

Wood, B. J. (1988). Activity measurements and excess entropy–volume relationships for pyrope–grossular garnets. *Journal of Geology* **96**, 721–729.

Wood, B. J. (1990). An experimental test of the spinel peridotite oxygen barometer. *Journal of Geophysical Research* **95**, 15845–15851.

Wood, B. J. & Kleppa, O. J. (1984). Chromium–aluminum mixing in garnet: A thermochemical study. *Geochimica et Cosmochimica Acta* **48**, 1373–1375.

Wood, B. J., Bryndzia, T. & Johnson, K. E. (1990). Mantle oxidation state and its relationship to tectonic environment and fluid speciation. *Science* **248**, 337–345.

Woodland, A. B. & Koch, M. (2003). Variation in oxygen fugacity with depth in the upper mantle beneath the Kaapvaal craton, Southern Africa. *Earth and Planetary Science Letters* **214**, 295–310.

Woodland, A. B. & O'Neill, H. St. C. (1993). Synthesis and stability of $Fe^{2+}{}_3Fe^{3+}{}_2Si_3O_{12}$ garnet and phase relations with $Fe_3Al_2Si_3O_{12}$–$Fe^{2+}{}_3Fe^{3+}{}_2Si_3O_{12}$ solutions. *American Mineralogist* **78**, 1002–1015.

Woodland, A. B. & Peltonen, P. (1999). Ferric iron contents of garnet and clinopyroxene and estimated oxygen fugacities of peridotite xenoliths from the Eastern Finland Kimberlite Province. In: Nixon, P. H. (ed.) *Proceedings of the 7th International Kimberlite Conference*. Cape Town: Red Roof Publishers, pp. 904–911.

Woodland, A. B. & Ross, C. R., II (1994). A crystallographic and Mössbauer spectroscopy study of $Fe_3{}^{2+}Al_2Si_3O_{12}$–$Fe_3{}^{2+}Fe_2{}^{3+}Si_3O_{12}$ (almandine–'skiagite') and $Ca_3Fe_2{}^{3+}Si_3O_{12}$–$Fe_3{}^{2+}Fe_2{}^{3+}Si_3O_{12}$ (andradite–'skiagite') garnet solid solutions. *Physics and Chemistry of Minerals* **21**, 117–132.

Woodland, A. B., Angel, R. J., Koch, M., Kunz, M. & Miletich, R. (1999). Equations of state for $Fe^{3+}Fe^{2+}Si_3O_{12}$ 'skiagite' garnet and Fe_2SiO_4–Fe_3O_4 spinel solid solutions. *Journal of Geophysical Research* **104**, 20049–20058.

Wyllie, P. J. & Huang, W.-L. (1976). Carbonation and melting reactions in the system CaO–MgO–SiO_2–CO_2 at mantle pressures with geophysical and petrological applications. *Contributions to Mineralogy and Petrology* **54**, 79–107.

Yaxley, G. M., Berry, A. J., Kamenetsky, V. S., Woodland, A. B. & Golovin, A. V. (2012). An oxygen fugacity profile through the Siberian Craton—Fe K-edge XANES determinations of $Fe^{3+}/\sum Fe$ in garnets in peridotite xenoliths from the Udachnaya East kimberlite. *Lithos* **140–141**, 142–151.

APPENDIX

Calculation of reaction (4)

At 1373 K the free energy of reaction (4)

$$ski = 5\ Fe + 3\ q + 3\ O_2$$

may be obtained from reaction (3)

$$ski + hc = alm + mt$$

for which $\Delta G_3 = -69{\cdot}3$ kJ, as explained in the text.

First the Gibbs energy of skiagite is derived from reaction (3) and data from Holland & Powell (2011) tabulated below;

$$G_{ski} = G_{alm} + G_{mt} - G_{hc} + 69{\cdot}3 = -5348{\cdot}8\ \text{kJ}.$$

The Gibbs energies for alm, mt, hc, q, O_2 at 1373 K are listed below, where HP11 is Holland & Powell (2011), HP90 is Holland & Powell (1990), RH is Robie & Hemingway (1995), HONA is Holmes *et al.* (1986).and give (using HP11) $\Delta G_4 = 5\ G_{Fe} + 3\ G_q + 3\ G_{O2} - G_{ski} = 969{\cdot}0$ kJ.

	G_{HP11} (kJ)	G_{HP90} (kJ)	G_{RH} (kJ)	G_{HONA} (kJ)
q	−1029·1	−1028·8	−1029·1	
Fe	−70·1	−70·0	−70·1	−70·4
O_2	−314·0	−314·0	−313·9	−314·4
mt	−1516·4	−1517·3	−1516·6	
alm	−6176·2	−6177·3		
hc	−2274·5	−2273·7		

Using the data in the older HP90 dataset yields an almost identical result ($\Delta G_4 = 970{\cdot}4$ kJ).

This is significantly different from the value for ΔG_4 (981·0 kJ) given by Woodland & O'Neill (1993) from the same starting point of $\Delta G_3 = -69{\cdot}3$ kJ. Repeating the calculation of Woodland & O'Neill (1993) using the data tabulated above (they used HONA for Fe & O_2, HP90 for all other phases) yields $\Delta G_4 = 967{\cdot}2$ kJ, very similar to the calculation using the new Holland & Powell (2011) dataset.

As can be seen in the table above, the dataset values of Holland & Powell (1990, 2011) are in very good agreement with those of Robie & Hemingway (1995) and Holmes *et al.* (1986) for phases with available calorimetric data.

Gudmundsson & Wood (1995) calculated the free energy of reaction (1) using the following equilibria:

$$ski = 5\ Fe + 3\ q + 3\ O_2 \quad (4)$$

$$fa = 2\ Fe + q + O_2 \quad (a)$$

$$fa + q = fs \quad (b)$$

with $\Delta G_1 = 2\ \Delta G_4 - 5\ \Delta G_a + \Delta G_b = 133{\cdot}3$ kJ (or log $K_1 = -5{\cdot}07$). However, using the correct value for ΔG_4 of 969·0 kJ in place of 981·0 kJ changes ΔG_1 by 24 kJ and hence log K_1 by 0·91 log units.

Garnet barometer equilibria

The following four reactions:

$$2\ ski = 4\ fa + fs + O_2 \quad (1)$$

$$2\ py + 2\ andr + 2\ fs = 2\ gr + 4\ fa + 3\ en + O_2 \quad (2)$$

$$2\ ski + fo = 5\ fa + en + O_2 \quad (11)$$

$$6\ ski + 2\ py = 2\ alm + 12\ fa + 3\ en + 3\ O_2 \quad (12)$$

have been calibrated on the basis of this work and the updated dataset of Holland & Powell (2011; see Table 1) and expressed as equations of the form $\Delta G = a + bT + cP + dT^2 + eP^2 + fPT$ in Joules, which reproduce the full calculations to within 100 J [or 300 J for (12)] over the range 0–100 kbar and 1300–1800 K.

	a	bT	cP	$d(10^3)T^2$	$e(10^2)P^2$	$f(10^2)PT$
(1)	344670	−163·36	858	−7·5577	−2·3764	−2·0898
(2)	339010	−164·59	829	−7·6931	−2·0380	−11·299
(11)	971930	−462·79	2141	−25·2302	−5·1024	−42·632
(12)	971930	−141·02	320	−8·1706	−1·2421	−35·412

Spinel barometer equilibria

The following three reactions:

$$2\ mt + 3\ fs = 6\ fa + O_2 \quad (13)$$

$$2\ mt + 3\ en = 3\ fa + 3\ fo + O_2 \quad (14)$$

$$2\ mt + 3\ en + 6\ hc = 6\ sp + 6\ fa + O_2. \quad (15)$$

have been calibrated from the updated dataset of Holland & Powell (2011) (see Table 1) and free energies (in Joules) expressed as equations of the same form as above, and are valid for the range 0–40 kbar and 1300–1800 K.

	a	bT	cP	$d(10^3)T^2$	eP^2	fPT
(13)	471793	−172·28	−763	3·0957	1·5013	−0·30644
(14)	489249	−169·80	−639	4·1382	1·6490	−0·083798
(15)	467590	−143·15	−414	13·081	1·2801	−0·1818

Log f_{O_2} values are given relative to the FMQ buffer, which is taken from O'Neill (1987) and pressure-corrected using the volumes from Holland & Powell (2011); the expression used is (with P in kbar and T in K)

$$\text{Log}f_{o_2}(\text{FMQ}) = (-587474 + 1584{\cdot}427\ T - 203{\cdot}3164\ T\ln T + 0{\cdot}09271T^2 + 1810P)/[8{\cdot}3144\ T\ln(10)].$$

Garnet mixing model

Garnets with formula $(Ca,Mg,Fe,Mn)_3(Al,Fe^{3+},Cr)_2Si_3O_{12}$ are here described with the following six independent end-members: gr ($Ca_3Al_2Si_3O_{12}$), alm ($Fe_3Al_2Si_3O_{12}$), py

($Mg_3Al_2Si_3O_{12}$), sps ($Mn_3Al_2Si_3O_{12}$), uv ($Ca_3Cr_2Si_3O_{12}$) and ski ($Fe_3Fe^{3+}{}_2Si_3O_{12}$).

Five compositional variables are required to describe the variations in composition, and are taken as the site fractions on X and Y sites:

$x = X^X_{Fe}$, $c = X^X_{Ca}$, $m = X^X_{Mn}$, $f = X^Y_{Fe^{3+}}$, $z = X^Y_{Cr}$. This leads to the remaining two dependent site fractions as $X^X_{Mg} = 1 - x - c - m$, $X^Y_{Al} = 1 - z - f$.

The end-member proportions p_i, are given by

$$p_{py} = 1{-}x{-}c{-}m$$
$$p_{uv} = z$$
$$p_{ski} = f$$
$$p_{alm} = x{-}f$$
$$p_{gr} = c{-}z$$
$$p_{sps} = m.$$

The ideal activities may be written out using mixing-on-sites as

$$a_{py} = X^3_{Mg,X}X^2_{Al,Y} = (1{-}x{-}c{-}m)^3(1{-}z{-}f)^2$$
$$a_{uv} = X^3_{Ca,X}X^2_{Cr,Y} = c^3z^2$$
$$a_{ski} = X^3_{Fe,X}X^2_{Fe^{3+},Y} = x^3f^2$$
$$a_{alm} = X^3_{Fe,X}X^2_{Al,Y} = x^3(1{-}z{-}f)^2$$
$$a_{gr} = X^3_{Ca,X}X^2_{Al,Y} = c^3(1{-}z{-}f)^2$$
$$a_{sps} = X^3_{Mn,X}X^2_{Al,Y} = m^3(1{-}z{-}f)^2$$

and the non-ideal activity coefficients may be found from the macroscopic symmetric formalism as

$$RT\ln\gamma_a = -\sum_i\sum_{j>i}(p^0_i - p_i)(p^0_j - p_j)W_{ij}$$

in which p_k is the proportion of end-member, k, in the phase, p^0_k is the value of p_k in pure a, and W_{ij} is the macroscopic interaction parameter for the ij binary. The summations are over an independent set of end-members chosen to represent the composition of the phase. So, for example, the ski activity coefficient would be

$$\begin{aligned}RT\ln\gamma_{ski} = &-p_{py}p_{alm}W_{py,alm} - p_{py}p_{gr}W_{py,gr}\\ &-p_{py}p_{sps}W_{py,sps} - p_{py}p_{uv}W_{py,uv}\\ &+p_{py}(1-p_{ski})W_{py,ski} - p_{alm}p_{gr}W_{alm,gr}\\ &-p_{alm}p_{sps}W_{alm,sps} - p_{alm}p_{uv}W_{alm,uv}\\ &+p_{alm}(1-p_{ski})W_{alm,ski} - p_{gr}p_{sps}W_{gr,sps}\\ &-p_{gr}p_{uv}W_{gr,uv} + p_{gr}(1-p_{ski})W_{gr,ski}\\ &-p_{sps}p_{uv}W_{sps,uv} + p_{sps}(1-p_{ski})W_{sps,ski}\\ &+p_{uv}(1-p_{ski})W_{uv,ski}\end{aligned}$$

and, for the dependent end-member andr (≡ gr + ski − alm), the activity may be simply determined from

$$RT\ln a_{andr} = RT\ln a_{gr} + RT\ln a_{ski} - RT\ln a_{alm} - \Delta G_{(7)}$$

where $\Delta G_{(7)} = 53{\cdot}8 + 0{\cdot}0017T - 0{\cdot}068P$ kJ (see text).

Garnet mixing energies

For garnet mixing, the within-site and reciprocal energy terms used are given below (units kJ, K, kbar) including references (lower-case roman numerals) to their derivation.

$$W_{MgCaX} = 40{-}0{\cdot}012T{-}0{\cdot}10P \quad \text{(i)}$$
$$W_{FeCaX} = 4 + 0{\cdot}10P \quad \text{(ii)}$$
$$W_{MgFeX} = 4 + 0{\cdot}01P \quad \text{(iii)}$$
$$W_{MgMnX} = 9 + 0{\cdot}04P \quad \text{(iv)}$$
$$W_{MgCaX} = 0 + 0{\cdot}06P \quad \text{(v)}$$
$$W_{FeMnX} = 2 + 0{\cdot}02P \quad \text{(vi)}$$
$$W_{Fe3AlY} = 2 \quad \text{(vii)}$$
$$W_{CrAlY} = 2 \quad \text{(viii)}$$
$$W_{CrFe3Y} = 2 \quad \text{(ix)}$$
$$W_{CaAlMgFe3XY} = -\,53{\cdot}8 - 0{\cdot}0017T + 0{\cdot}068P \quad \text{(x)}$$
$$W_{CaAlFeFe3XY} = -\,53{\cdot}8 - 0{\cdot}0017T + 0{\cdot}068P \quad \text{(x)}$$
$$W_{CaAlMnFe3XY} = -\,30 + 0{\cdot}03P \quad \text{(x)}$$
$$W_{CaAlMgCrXY} = 10{\cdot}2 - 0{\cdot}0338T + 0{\cdot}121P \quad \text{(x)}$$
$$W_{CaAlFeCrXY} = 10{\cdot}2 - 0{\cdot}0338T + 0{\cdot}121P \quad \text{(x)}$$
$$W_{CaAlMnCrXY} = -\,30 + 0{\cdot}03P. \quad \text{(x)}$$

The within-site terms refer to mixing of three cations on X sites and two cations on Y sites. The references for the within-site terms are as follows: (i) symmetric fit to the Ca-poor half of the binary data of Newton *et al.* (1977), Wood (1988) and Ganguly *et al.* (1996); (ii) Geiger *et al.* (1987), Koziol (1990); (iii) Geiger *et al.* (1987), Hackler & Wood (1989) and Koziol & Bohlen (1992); (iv) Davies & Navrotsky (1983) and Ganguly *et al.* (1996); (v) Koziol (1990); (vi) Pownceby *et al.* (1987); (vii) Holland & Powell (2011) based on fitting measured $Fe^{3+}/(Fe^{3+}+Al)$ ratios of garnet in experiments of Holdaway (1972) for coexisting garnet + anorthite + wollastonite + quartz; (viii) Mattioli & Bishop (1984) and Wood & Kleppa (1984); (ix) taken as the same as W_{Fe3AlY}; (x) this study.

The cross-site terms are determined here as follows. $W_{CaAlFeFe3XY}$ comes from the discussion in the text and uses our free energy of skiagite in conjunction with the data of Holland & Powell (2011). It should be noted that

the cross-site *W*s here have opposite sign to the free energies of the reactions in the text. $W_{CaAlMgFe3XY}$ is made identical to $W_{CaAlFeFe3XY}$ as done by Gudmundsson & Wood (1995) and is equivalent to assuming a zero energy for FeFe + MgAl = MgFe + FeAl. This latter was estimated by Ottonello *et al.* (1996) as a small value, within error of zero on inspection of their other estimates. A value for $W_{CaAlMgCrXY}$ was determined from the updated Holland & Powell (2011, see Table 1) dataset, and that for $W_{CaAlFeCrXY}$ was taken to be identical. The two cross-site terms involving Mn are given much smaller values based on the fact that calderite $Mn_3Fe^{3+}{}_2Si_3O_{12}$ is stable to much lower pressures (it is found in natural blueschists) than knorringite or skiagite. Oxybarometry is not sensitive to $W_{CaAlMgCrXY}$, $W_{CaAlFeCrXY}$, or the Mn cross-site terms.

This set allows us to determine the complete set of macroscopic *W*s presented in the text, using the relations given below.

$$W_{py,gr} = W_{MgCaX}$$
$$W_{py,alm} = W_{MgFeX}$$
$$W_{py,sps} = W_{MgMnX}$$
$$W_{py,uv} = -W_{CaAlMgCrXY} + W_{CrAlY} + W_{MgCaX}$$
$$W_{py,ski} = W_{CaAlFeFe3XY} - W_{CaAlMgFe3XY} + W_{Fe3AlY} + W_{MgFeX}$$
$$W_{gr,alm} = W_{FeCaX}$$
$$W_{gr,sps} = W_{MnCaX}$$
$$W_{gr,uv} = W_{CrAlY}$$
$$W_{gr,ski} = W_{CaAlFeFe3XY} + W_{Fe3AlY} + W_{FeCaX}$$
$$W_{alm,sps} = W_{FeMnX}$$
$$W_{alm,uv} = -W_{CaAlFeCrXY} + W_{CrAlY} + W_{FeCaX}$$
$$W_{alm,ski} = W_{Fe3AlY}$$
$$W_{sps,uv} = W_{CaAlFeFe3XY} - W_{CaAlMnFe3XY} + W_{Fe3AlY} + W_{FeMnX}$$
$$W_{uv,ski} = -W_{CaAlFeCrXY} + W_{CaAlFeFe3XY} + W_{CrFe3Y} + W_{FeCaX}.$$

When considering andradite, the additional *W* terms used in the text are defined as

$$W_{alm,andr} = -W_{CaAlFeFe3XY} + W_{Fe3AlY} + W_{FeCaX}$$
$$W_{py,andr} = -W_{CaAlMgFe3XY} + W_{Fe3AlY} + W_{MgCaX}$$
$$W_{andr,uv} = W_{CrFe3Y}$$
$$W_{gr,andr} = W_{Fe3AlY}$$
$$W_{sps,andr} = -W_{CaAlMnFe3XY} + W_{Fe3AlY} + W_{MnCaX}$$
$$W_{andr,ski} = W_{FeCaX}.$$

Orthopyroxene mixing

Orthopyroxene non-ideality has only minimal impact on garnet oxybarometry, but affects the spinel barometers significantly, raising the typical calculated log f_{O_2} for reaction (13) by around 0·2 log units. Here we modify the mixing model of Green *et al.* (2012) and Jennings & Holland (2015), simplifying it by making it symmetric, by ignoring Fe–Mg ordering between M2 and M1 sites and by taking all non-ideal interactions as contributed only by the end-members en, fs, di, mgts. The di end-member refers to orthorhombic diopside ($CaMgSi_2O_6$) and mgts to Mg-Tschermak pyroxene ($MgAlAlSiO_6$).

For the en and fs end-members the ideal activities are given by

$$a_{en}^{ideal} = X_{Mg}^{M2} X_{Mg}^{M1} (X_{Si}^{T})^{1/2} \text{ and } a_{fs}^{ideal} = X_{Fe}^{M2} X_{Fe}^{M1} (X_{Si}^{T})^{1/2}.$$

The powers of $\frac{1}{2}$ (rather than two) come about because the entropy of mixing on the tetrahedral sites is taken as a quarter that of full disorder, to help mimic short-range order between M and T sites (Green *et al.*, 2012). Non-ideality is expressed as a regular solution, as discussed above for garnet, with the following parameters (in kJ):

$$W_{fs,en} = 2{\cdot}0$$
$$W_{fs,mgts} = 7{\cdot}0 - 0{\cdot}15P$$
$$W_{fs,di} = 24{\cdot}0$$
$$W_{en,mgts} = 13{\cdot}0 - 0{\cdot}15P$$
$$W_{en,di} = 32{\cdot}2 + 0{\cdot}12P$$
$$W_{mgts,di} = 75{\cdot}0 - 0{\cdot}94P.$$

Olivine mixing

Olivine mixing is represented as in Gudmundsson & Wood (1995), with ideal activities for fo and fa given as

$$a_{fo}^{ideal} = X_{Mg}^{M2} X_{Mg}^{M1} \text{ and } a_{fa}^{ideal} = X_{Fe}^{M2} X_{Fe}^{M1}$$

and non-ideality expressed as a regular solution, taking $W_{fo,fa} = 7{\cdot}4$ kJ (Gudmundsson & Wood, 1995).